

## Article

# Full-Scale Blast Tests on a Conventionally Designed Three-Story Steel Braced Frame with Composite Floor Slabs

Michalis Hadjioannou <sup>1,\*</sup>, Aldo E. McKay <sup>2</sup> and Phillip C. Benshoof <sup>3</sup><sup>1</sup> Applied Research, Protection Engineering Consultants, Dripping Springs, TX 78620, USA<sup>2</sup> Protective Design, Protection Engineering Consultants, San Antonio, TX 78213, USA; amckay@protection-consultants.com<sup>3</sup> Bureau of Diplomatic Security, U.S. Department of State, Arlington, VA 22209, USA; benshoofpc@state.gov

\* Correspondence: mhadjioannou@protection-consultants.com

**Abstract:** This paper summarizes the findings of two full-scale blast tests on a steel braced frame structure with composite floor slabs, which are representative of a typical office building. The aim of this research study was to experimentally characterize the behavior of conventionally designed steel braced frames to blast loads when enclosed with conventional and blast-resistant façade. The two tests involved a three-story, steel braced frame with concentric steel braces, which are designed to resist typical gravity and wind loads without design provisions for blast or earthquake loads. During the first blast test, the structure was enclosed with a typical, non-blast-resistant, curtainwall façade, and the steel frame sustained minimal damage. For the second blast test, the structure was enclosed with a blast-resistant façade, which resulted in higher damage levels with some brace connections rupturing, but the building did not collapse. Observations from the test program indicate the appreciable reserved capacity of steel brace frame structures to resist blast loads.

**Keywords:** steel structure; steel frame; composite floor; steel braces; blast loads; blast-resistant design; curtainwall façade



**Citation:** Hadjioannou, M.; McKay, A.E.; Benshoof, P.C. Full-Scale Blast Tests on a Conventionally Designed Three-Story Steel Braced Frame with Composite Floor Slabs. *Vibration* **2021**, *4*, 865–892. <https://doi.org/10.3390/vibration4040049>

Academic Editors:  
Christoforos Dimopoulos and Charis J. Gantes

Received: 29 September 2021  
Accepted: 21 November 2021  
Published: 24 November 2021

**Publisher's Note:** MDPI stays neutral with regard to jurisdictional claims in published maps and institutional affiliations.



**Copyright:** © 2021 by the authors. Licensee MDPI, Basel, Switzerland. This article is an open access article distributed under the terms and conditions of the Creative Commons Attribution (CC BY) license (<https://creativecommons.org/licenses/by/4.0/>).

## 1. Introduction

As a result of past terrorist attacks, such as the Alfred P. Murrah Building in Oklahoma City in 1995 and the attacks against the World Trade Center in New York City in 2001, researchers have been working to enhance the physical security of buildings in order to protect human lives and infrastructure. As such, many important buildings require consideration of blast loads in their design. Blast pressures can be man-made or accidental. A required feature of blast-resistant buildings is the use of hardened envelope façade systems. Their primary function during a blast event is to protect occupants from direct exposure to the blast wave, blast-induced debris from failure of the external envelope of the building (breakup of window glass, exterior, and interior walls), and free-fall injuries in case they are ejected from elevated floors [1]. While the performance levels of hardened façade envelopes vary depending on the material they are made of and the required level of protection [2], in general, they are designed to plastically deform but not to detach and penetrate into the building, thereby protecting occupants.

Hardened building envelopes are designed to absorb the applied blast load through elastic and plastic deformation; they generally collect a relatively high portion of the total applied blast load impulse. Then, the blast load absorbed from the façade is transferred to the structural frame of the building as dynamic reactions through the supporting diaphragm, beams, and columns. Depending on the design basis threat, the lateral-force-resisting system (LFRS) of the building is designed accordingly to resist these loads by following the generally acceptable approach of balanced or capacity design [3]. Generally, the structural frame of reinforced concrete and steel frame buildings that are designed

and detailed for seismic loads tend to perform better under blast loads because of their increased ductility [4,5].

Nonetheless, a concern is raised for the LFRS of existing buildings that have not been designed to resist a design-basis blast threat nor designed for seismic loads. This may be the case for older buildings when retrofitted with hardened, blast-resistant façade systems. Generally, in this situation, cast-in-place reinforced concrete structures are known to perform better under blast loads due to their higher mass and monolithic construction [6]. Conversely, steel frame buildings are of higher concern due to lack of available data for their global response to blast loads. Their relatively lower mass and lack of ductility can negatively affect their response. In such buildings, their LFRS may need to be retrofitted accordingly [1] by applying the balanced design philosophy to ensure that the higher resistance of the façade will not overload the LFRS, thereby compromising the structural integrity of the building.

To date, research studies investigating the response of steel frame buildings to blast have primarily focused on the response of isolated components under short-duration blast loads that are likely to only cause localized damage to one or few columns, which can potentially trigger progressive collapse [5,7] similar to the partial collapse of the Alfred P. Murrah Building in Oklahoma City in 1995. In that context, many studies have investigated the response of isolated steel members numerically [8–10] and with simulated or actual blast tests [5,11–13].

However, evaluation of the response of buildings under relatively long duration blast loads where the blast overpressure is expected to globally load the building with a nearly uniform load distribution on the building envelope [14] are mostly computational and sparse. In addition, most of these studies have focused on the response of strengthened structures by means of improved connection details and/or hardened members. Recently, Yussoft et al. [15] evaluated numerically the response of steel frames with strengthened joints, while Weli and Vigh [16] evaluated the response of a special self-centering steel moment frame (SMF) showing that such frames can reduce the residual drift after a blast event. Nourzadeh et al. [17] demonstrated computationally that the lateral story drifts on a 10-story seismically designed reinforced concrete (RC) building subjected to moderate blast loads resulting from a 1000 kg TNT charge at standoff distances between 15 and 30 m can be significantly larger than those observed as a result of earthquake ground motions for selected cities in the eastern and western regions of Canada. Ibrahim and Nabil [18] also investigated the response of an RC frame to blast loads and concluded that when columns were designed to have higher ductility, the building's response was significantly improved.

Studies on the response of conventionally designed buildings with no seismic or blast-resistant design considerations under larger-duration blast loads are limited. For this reason, the U.S. Department of State (DoS) Bureau of Diplomatic Security, in collaboration with research partners from Protection Engineering Consultants and the Energetic Materials & Testing Center (EMRTC) of the New Mexico Tech, directed and funded a multi-year research program focusing on characterizing the response of conventional steel frame buildings to blast loads.

Under this program, McKay et al. [19] performed a comprehensive analytical study on the blast response of common types of steel frame buildings with different numbers of stories and different types of LFRSs, namely SMF and steel braced frames (SBF). The analytical study results suggest that buildings with non-blast-resistant façade envelopes that are expected to fail early under blast while posing a significant hazard to building occupants due to failed debris are not prone to collapse, since the rapid failure of the façade limits the peak applied lateral load to the building's frame. Therefore, damage to their LFRS is not expected. Conversely, the lateral load demand on the LFRS of these conventional buildings enclosed with a blast-resistant façade is higher due to the façade's ability to absorb and transfer a larger portion of the applied blast load to the LFRS without failing. The study also showed that steel buildings of 12 stories or more with hardened envelopes are not prone to collapse due to their increased stiffness needed for wind serviceability,

while there was strong evidence that buildings with less than three stories were vulnerable to severe damage on the LFRS, which could lead to total collapse.

Mid-rise steel frames with three to six stories were found to be more susceptible to localized damage on their LFRS, but their safety margin against collapse was unclear [19]. This finding motivated the full-scale blast test program presented in this paper, which focused on experimentally testing the response against relatively long duration blast loads of a three-story steel frame building that was designed to only resist typical gravity and wind loads with a basic wind speed of 51 m/s. No provisions for blast or seismic loads were considered for the design of the LFRS of the test structure. Two tests were performed. During the first test, the building was enclosed with a conventional curtainwall glazed façade, and during the second test, the building was enclosed with a blast-resistant façade. The applied blast loads were similar for both tests. During the first test, the frame responded elastically with no failure on the LFRS, while the glazed façade almost completely shattered. The blast-resistant façade on the second test collected a higher portion of the blast load and transferred it to the LFRS, which resulted in partial compromise of the LFRS. Some first-floor gusset plate connections completely ruptured, and some others yielded but did not fail. Despite the partial damage of the LFRS, the frame had a residual permanent lateral deformation at the roof level of less than 3 mm, indicating that there was an appreciable margin of safety against collapse.

## 2. Problem Statement, Scope, and Objectives

A question is raised when existing buildings, especially steel frame structures, are retrofitted with blast-resistant façades to meet physical security requirements as to whether their LFRS should also be retrofitted. This is particularly true in cases where the LFRS is designed only to resist typical gravity and wind loads with no seismic detailing or blast load considerations. This research study focused on characterizing the behavior of conventional steel structures subjected to relatively high-magnitude, long-duration blast loads that can globally load the building envelope with approximately uniform blast pressures. Such blast loads can potentially result in the global sway response of the structure, causing the localized damage of key structural members up to complete collapse. Although not presented in this paper, another objective of the test series was to identify key factors to consider for assessments of existing buildings and simplified structural analysis methods for evaluating the performance of steel frame buildings under blast loads. The structural analysis methods were derived from the experimental data with the intent of allowing for efficient yet accurate modeling of buildings in response to blast loads using conventional structural analysis software. This will be a topic of a future publication.

## 3. Description of Three-Story Steel Frame Test Structure

The test structure designed for this research program was a full-scale, three-bay  $\times$  two-bay three-story steel frame with typical square bays, 6.10 m long. It was constructed at the field laboratory of the EMRTC in Socorro, NM. The frame's story height was 4.10 m and comprised of steel-concrete composite floors. Figure 1a,b show the typical floor and roof plan of the test frame, respectively. The LFRS consisted of concentric steel braces, which are commonly known as chevron braces. The building had two sets of chevron braces per floor parallel to the 12.20 m long side along gridlines B and C, which are shown in Figure 2a. Along the 18.30 m long side, there was one set of braces per floor along gridline 2, as shown in Figure 2b. The LFRS was designed to resist typical wind loads without provisions for resisting earthquake or blast loads. For the first blast test, the frame was enclosed by a conventional glazed curtainwall facade. For the second blast test, the façade enclosure was replaced with a hardened (blast-resistant) façade, which was designed to plastically deform but not rupture the applied blast load.

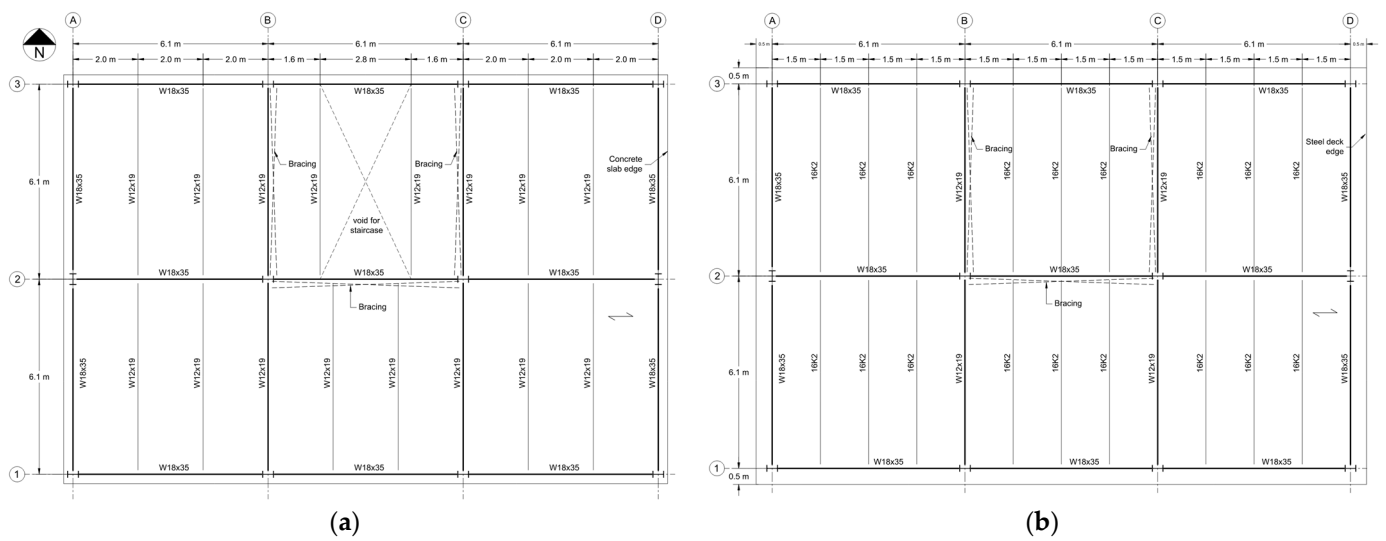


Figure 1. Test structure plan views: (a) 2nd and 3rd floor (typical); (b) Roof.



Figure 2. LFRS of test structure: (a) Braces along gridlines B and C, looking east (typical); (b) Braces along gridline 2, looking north.

### 3.1. Choice of Test Structure

The choice of this particular steel structure type and number of stories was informed from an earlier extensive analytical study by McKay et al. [19]. This study focused on numerically assessing the performance of different types of steel buildings to far-field, long duration, blast loads. For the study, conventionally designed steel buildings with the two most common categories of LFRS, (a) steel braced frames (SBF) (concentric, eccentric, cross-braced) and (b) SMF, were included. In summary, the findings of the study suggested that as the number of stories increases, the collapse potential due to blast loads drops. In addition, most steel structure types that are enclosed with conventional (non-blast-resistant) façades are not prone to collapse due to the early failure of fragile façade systems such as non-blast-resistant glazing. Conversely, the load demand on the LFRS of steel frame buildings with a hardened façade is higher because a non-failing façade collects a higher portion of the blast load that is eventually transferred to the LFRS of the building.

Among the different LFRS types that were included in the study [19], the most vulnerable type was SBFs. Buildings with less than three stories were found to be the worst performing ones, since they were vulnerable to severe damage during blast events. Conversely, buildings of 12 stories (or more) were not prone to collapse. However, mid-rise SBFs i.e., 3 to 6 stories, were found to be susceptible to localized damage on the LFRS, but their safety margin against collapse was unclear. Thereby, for the current test program, it

was decided to use a 3-story SBF that was designed for conventional loads i.e., gravity and typical wind load with a basic wind speed of 51 m/s as a test structure. Its LFRS was comprised of concentric steel braces (chevron), which constituted one of the most vulnerable brace configurations among those considered in the study [19], i.e., cross bracing, eccentric bracing, and concentric bracing.

### 3.2. Design of Test Structure

The test structure was designed to represent a typical office building. The design loads were based on ASCE/SEI 7-10 [20]. For strength and serviceability, the building was designed to meet the requirements of AISC 360-10 [21]. The dead load due to the self-weight of the slab and steel members was  $2.3 \text{ kN/m}^2$ , and an additional dead load of  $0.5 \text{ kN/m}^2$  was assumed to account for permanent floor loads. The design floor live load was  $4.8 \text{ kN/m}^2$ , resulting in an ultimate design load (UDL) ( $1.2 \times \text{dead} + 1.6 \times \text{live}$ ) of  $11.0 \text{ kN/m}^2$ .

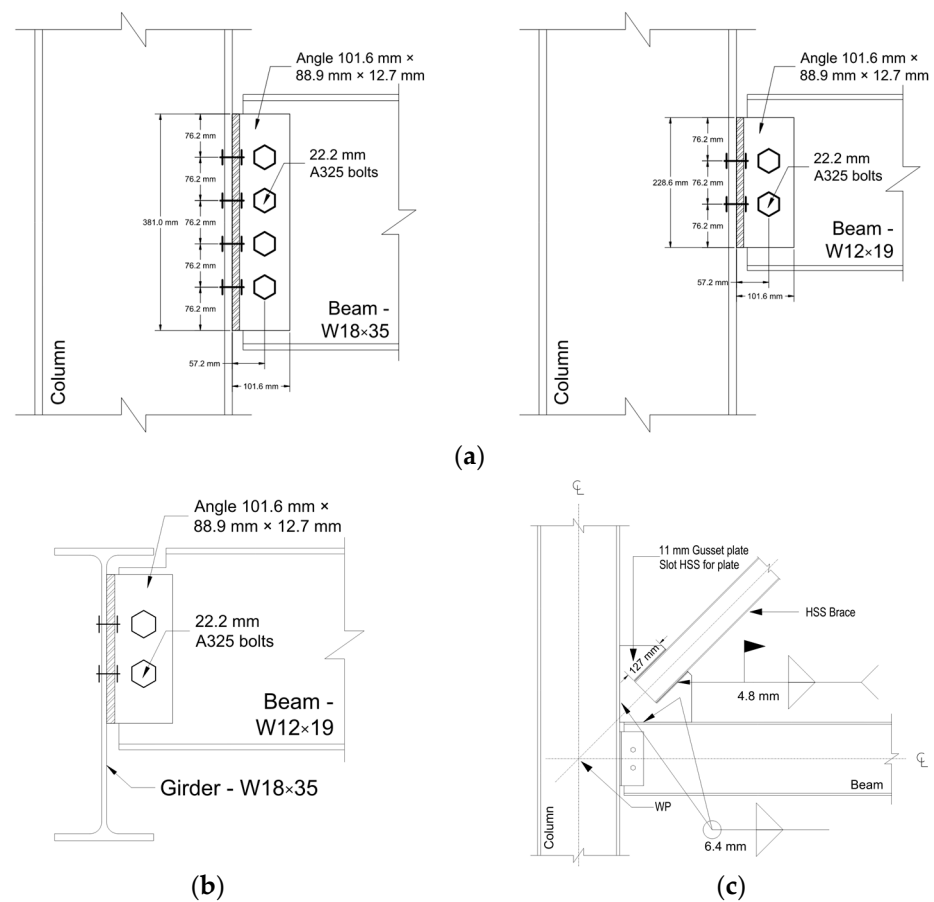
Figure 1a shows a plan view of the second and third floor with the member sizes that were used. The columns were on a 6.10 m long square grid forming three bays in the East–West (EW) direction and two bays on the North–South (NS) direction. Each bay had two intermediate floor beams at the third points along the NS direction. All spandrel beams were  $W18 \times 35$  as well as the intermediate girders on the EW direction. All intermediate beams in the NS direction were  $W12 \times 19$ . All steel beams acted compositely with a 114 mm thick normal-weight ( $24 \text{ kN/m}^2$ ) concrete slab that was poured over a 20-gauge galvanized composite metal decking with 51 mm deep corrugations that were parallel to the EW direction. The composite action between steel beams and concrete slab was facilitated through 19.1 mm diameter, 89 mm long shear studs. Shear studs had a 300 mm spacing and were placed at each low flute of the metal decking. The slab had 12.7 mm diameter reinforcing bars in both directions, which were placed 19 mm below the top of the concrete slab.

Figure 1b shows the roof layout that was designed for a live load of  $1.0 \text{ kN/m}^2$ . The beam sizes spanning between columns were the same size as those of the floors below. Each bay had three intermediate open-web steel joists at the quarter points along the NS direction, size 16K2. The roof frame was covered with a 38 mm deep, 19-gauge galvanized roof deck type “B” per the Vulcraft product catalogue [22].

The story height was 4.10 m, and all columns were  $W14 \times 43$ , extending over the full height of the building. The LFRS was designed to resist a typical wind load with a basic wind speed of 51 m/s for strength and 40 m/s for serviceability for a maximum inter-story drift of  $h/400$ , where  $h$  is the story height. Earthquake or blast loads were not considered. Figure 1 indicate the locations of the chevron braces. Specifically, along the NS direction, they were two sets of braces per floor, one at each interior column line (gridlines B and C). Likewise, along the EW direction, one brace line was used at the interior column line (gridline 2). All braces were made of square hollow structural sections (HSS). Their sizes at each floor and at each direction are indicated in Figure 2.

### 3.3. Structural Connection Details

All beam-to-column connections were bolted with double angles using 22 mm diameter bolts at both legs, as shown in Figure 3a. All floor-beam-to-girder connections were also using bolted double angles with two 22 mm diameter bolts as shown in Figure 3b. All brace connections were welded using a 11 mm thick gusset plate, as shown in Figure 3c. The ends of the HSS brace members were slotted and inserted into the gusset plate such that all four contact edges were fillet welded to the gusset plate with a 4.8 mm fillet weld, resulting in a total weld length per joint of 508 mm ( $4 \times 127 \text{ mm}$ ). All columns were connected to the concrete foundation with typical base plate connections using four 22 mm diameter cast-in-place anchor rods.



**Figure 3.** Details of structural connections between steel members: (a) Beam-to-column joints; (b) Girder-to-beam joint; (c) Gusset plate brace connection.

### 3.4. Material Properties

All wide flange columns and beams were made of ASTM A992 steel [23]. The braces were made of ASTM A500 Grade B steel [24]. The clip angles for the joints were made of ASTM A36 steel [25], while the deck utilized ASTM A653, Grade 33 steel [26]. All bolts for the steel frame joints were ASTM A325 [27], and all welds were made with E70 electrodes. The 28-day cylinder compressive strength of all concrete (foundation, slab on grade, floor slabs) was 28 Mpa, and the cast-in-place anchor rods used for the column base plate connections had a 720 MPa specified yield stress. Finally, all reinforcing bars were made of ASTM A615, Grade 60 steel [28].

### 3.5. Conventional Façade Details

For the purposes of the first blast test, the steel frame was enclosed in all four elevations with a conventionally designed, non-blast-resistant, curtainwall glazed façade. The façade was designed to conform with the requirements of IBC 2006 [29] for a basic wind speed of 40 m/s for serviceability and 51 m/s for strength. The façade comprised of vertically spanning aluminum mullions connected at each floor level with a 1.2 m horizontal spacing, as shown in Figure 4a. Over the 12.3 m height of the building, six insulated glass units (IGU) were used. The IGU panels had a nominal thickness of 25.4 mm and were made with non-laminated tempered glass; 6.35 mm glass | 12.7 mm airspace | 6.35 mm glass. All mullions (horizontal and vertical) were 190 mm deep and 63.5 mm wide based on the Kawneer “1600 Wall System<sup>®</sup>1 Curtain Wall” [30]. A view of the typical cross-section of the vertical and horizontal mullions are shown in Figure 4b. The vertical mullions were attached to the webs of the W18 × 35 spandrels at each floor level with kicker members shown in Figure 4c.

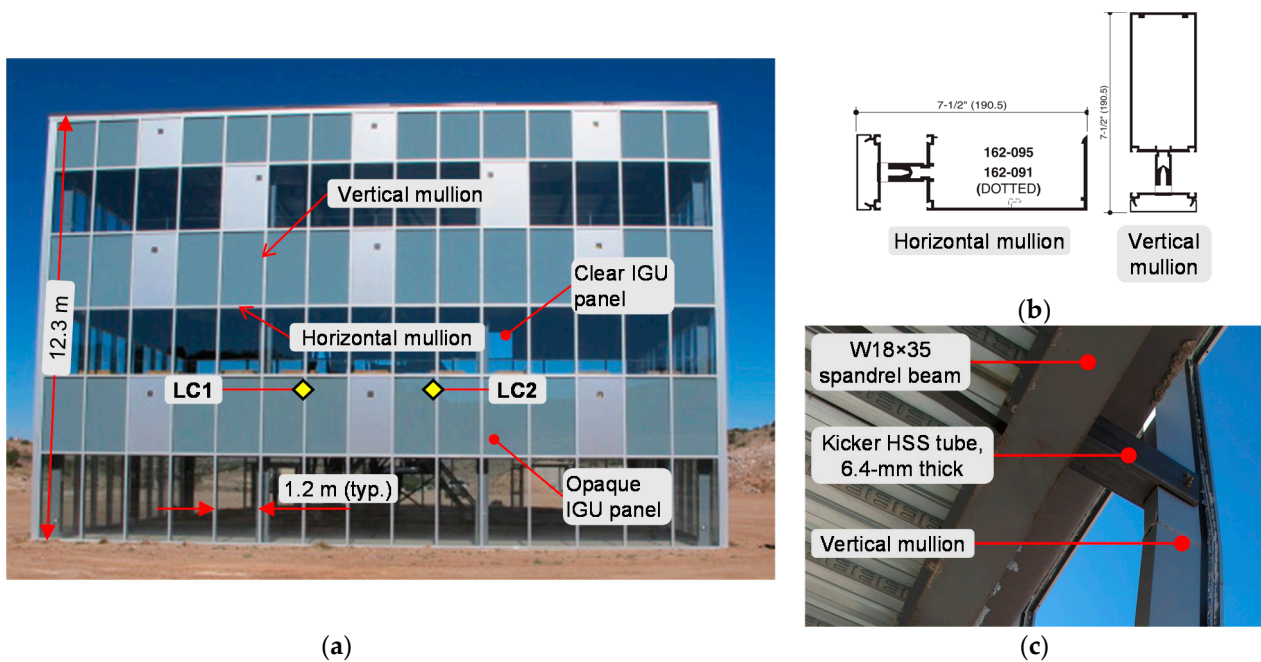


**Figure 4.** View of the test structure with conventional curtainwall glazed façade used for Test 1: (a) South elevation view (LC = load cell, refer to Figure 9a); (b) Horizontal and vertical mullion cross-sections; (c) Vertical mullion-to-spandrel beam connection with kickers.

### 3.6. Blast-Resistant Façade Details

For the purposes of the second blast test, a blast-resistant façade was used to enclose the test structure at all four elevations. Due to budget restrictions, instead of a blast-resistant glazed curtainwall façade with aluminum mullions, a steel façade was used. The steel façade was designed to meet similar strength and performance requirements as the equivalent aluminum glazed one with similar mass. Specifically, the façade system was designed for a low-level-of-protection (LLOP) per PDC-TR 06-08 [2], which allows permanent plastic deformation, but not rupture, preventing debris with significant velocities to enter the building and cause serious injuries or fatalities. For the 4.10 m floor height of the test frame herein, the maximum allowable deflection was 215 mm.

A view of the test structure with the steel façade is shown on Figure 5a. The blast-resistant steel façade comprised vertical  $MC7 \times 22.7$  steel channels, made with A36 steel [25], spanning between floors, with an on-center spacing of 610 mm, as indicated in Figure 5b. At the first floor, the steel channels were covered with a 16 mm thick A36 steel plate that was welded to the exterior flange of the channels. The channels on the second and third floor were covered with horizontally spanning, 38 mm deep, 16-gauge galvanized deck type “B” per the Vulcraft® product catalogue [22] that was fastened to the channels with self-tapping screws spaced at 300 mm. It is noted that a 16 mm thick plate on the first story was used, instead of the steel deck, to meet the performance requirements for forced entry/ballistic resistant (FE/BR), which are typically required for some blast-resistant buildings at the first floor to protect against forced-entry attacks and ballistic threats.

As a result of its relatively high stiffness and strength, special attention was given to the connection details of this façade to the steel frame to avoid its participation in resisting lateral loads through shear-wall-type action. This requirement was facilitated by positively connecting the top ends of the  $MC7 \times 22.7$  steel channels with a bolted connection only. The bottom ends of the  $MC7 \times 22.7$  steel channels did not have any positive connection for gravity loads. Instead, they were in a track that allowed them to accommodate serviceability deflections and to slide as the building experienced sway motion and still be able to resist the applied blast loads via bearing-type action with the track. A close-up view of this connection is shown in Figure 5c.

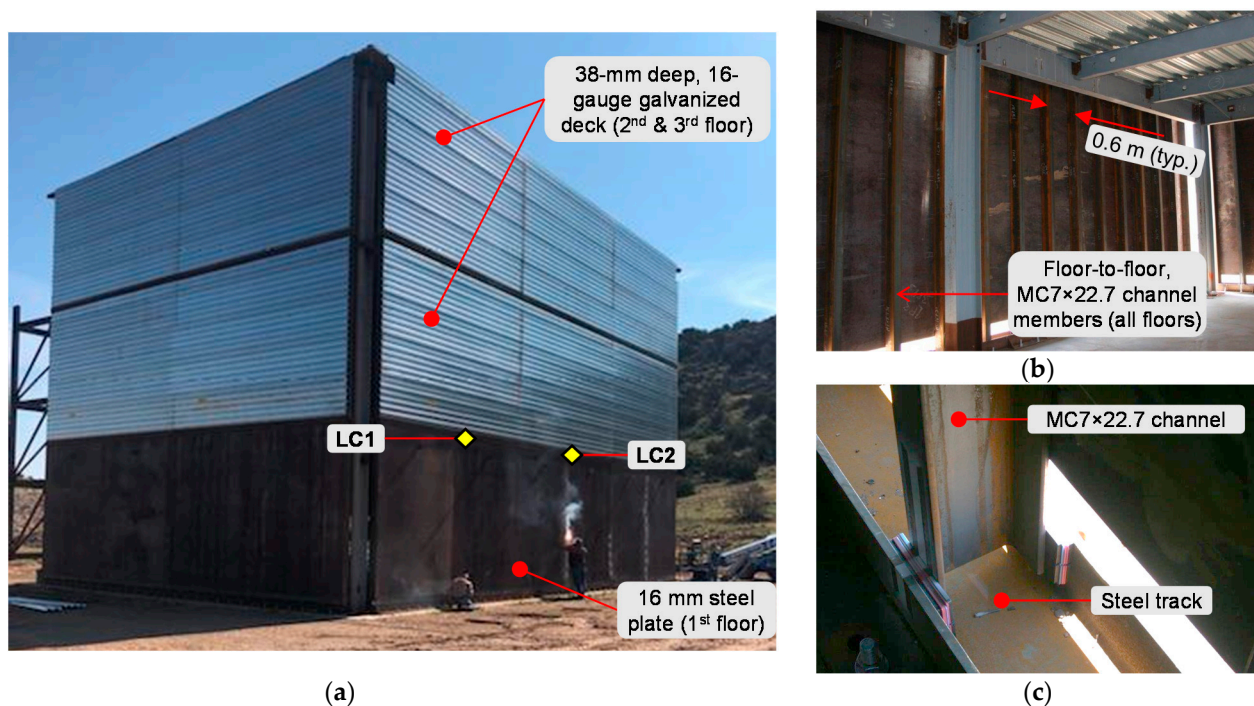


**Figure 5.** View of the test structure with blast-resistant steel façade for Test 2: (a) Southwest elevation view (LC = load cell, refer to Figure 9b); (b) View from the inside on the 1st floor (same channel configuration on all floors); (c) Close-up view of bottom end connection of  $MC7 \times 22.7$  façade channels to allow sliding for in-plane motion and resist load for out-of-plane motion.

### 3.7. Instrumentation

For both tests, a high-frequency data acquisition system was used with a sampling rate sufficient to capture a high-resolution signal from the various gauges that were attached to the test structure. All the recorded data were synchronized with the time of detonation of the explosive charge. Thereby, throughout this paper, the time axis on the recorded data is time after detonation. The instrumentation included the following types of sensors:

- Pressure gauges (PG);
- Displacement gauges (DG);
- Strain gauges (SG) on selected key elements of the LFRS;
- Load cells (LC) on some façade-to-structure connection points.

An array of eleven (11) PGs were mounted to the front elevation of the structure that was directly loaded from the airblast pressure to capture the reflected pressure and impulse profile, which are shown in Figure 6a. Another four (4) PGs were mounted to the roof and side elevation of the structure to measure the incident pressure, as shown in Figure 6b,c. Figure 6d shows the four (4) PGs that were attached on the first and second floor to measure the interior pressure.

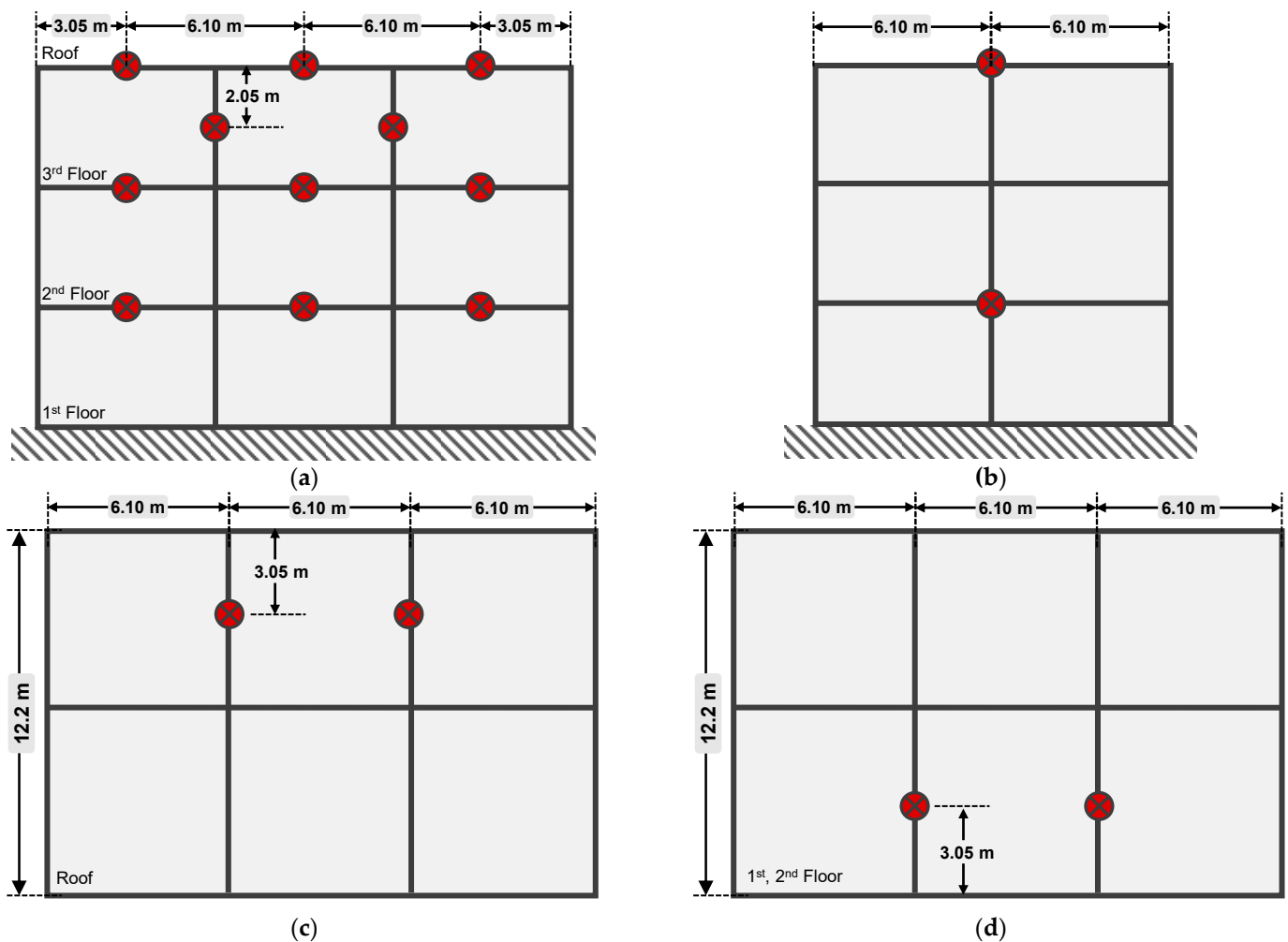


**Figure 6.** Pressure gauge locations on the test structure: (a) Front (south) elevation, directly loaded face; (b) Side (east and west) elevation; (c) Roof; (d) First and second floor (interior pressure gauges).

For redundancy, a total of nine (9) DGs, three (3) per floor level, were used to measure the lateral displacement history at each one of the three floor levels. All DGs were mounted to the back side of the structure i.e., the elevation opposite to the one directly loaded from the blast pressure. The DGs were placed at the floor levels and were mounted to a non-responding steel-frame instrumentation tower, which is shown in Figure 7.

For estimating the peak axial load on the chevron braces of the LFRS, a total of 24 SGs were attached to the two brace lines along the load direction (Figure 2a) i.e., braces along gridlines B and C. Specifically, a pair of two SGs were attached at each one of the 12 HSS brace members. Each SG pair was located at the midspan of each brace with the two SGs glued to the two opposite sidewalls of the HSS tube brace member. Figure 8 shows the locations and IDs of these SGs. More strain gauges were installed at other critical members such as columns and beams.



**Figure 7.** View of the instrumentation tower on the north (rear) elevation of the test structure indicating the locations of the displacement gauges (DG) at the three floor levels (same configuration on both tests).

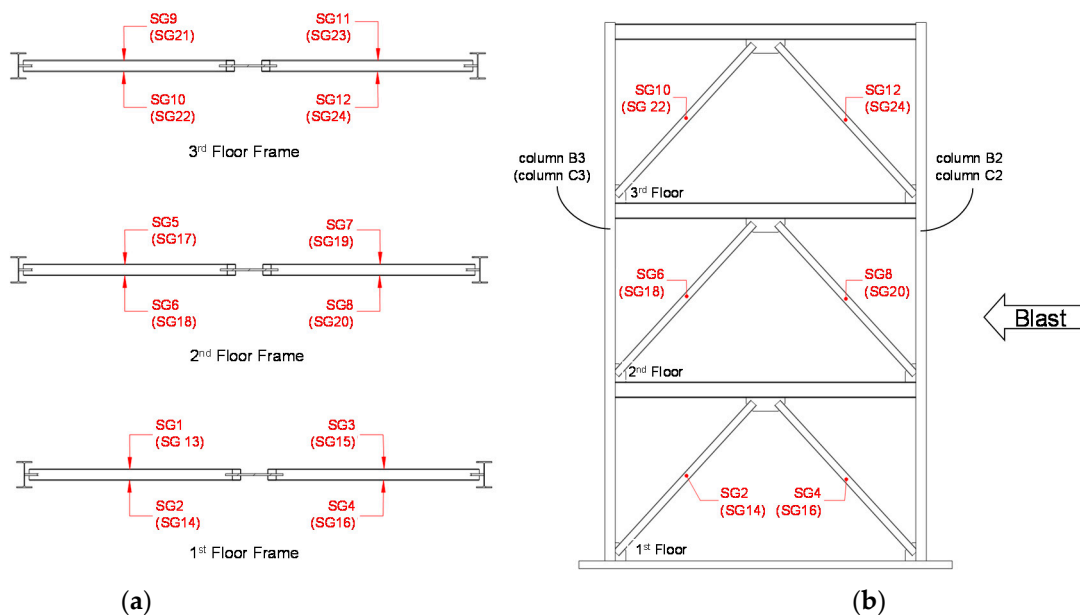


**Figure 8.** Strain gauge locations on braces along blast direction: (a) Plan view of braces per floor; (b) Side view of braces; IDs in brackets refer to strain gauges attached on column line C braces.

A few connection points of the façade to the steel frame were modified to accommodate LCs to directly measure the dynamic reaction load that the façade transferred to the building. The load cell locations for the first and second test are indicated in Figures 4a and 5a, respectively. The LCs were positioned at the second-floor level, as shown in Figure 9.

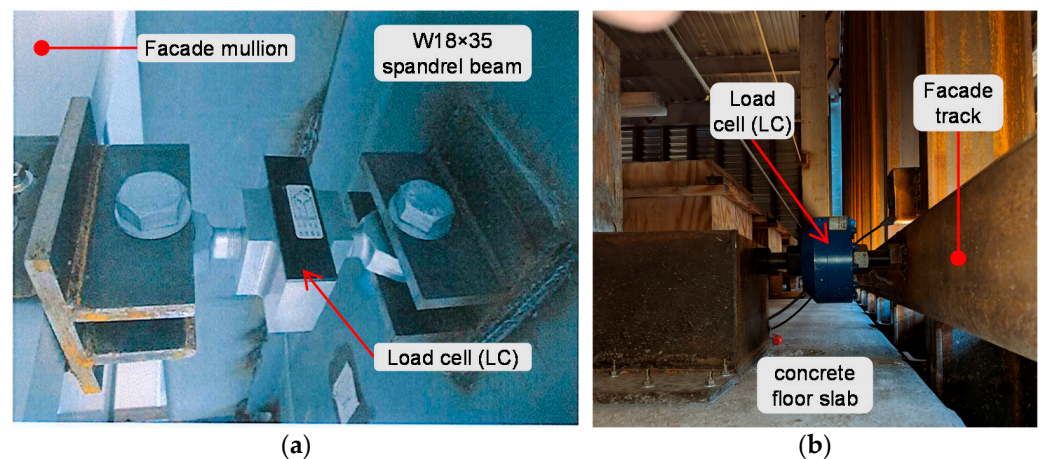


**Figure 9.** Close-up views of load cell configuration to measure the dynamic reaction loads transferred from the façade to the steel frame: (a) Test 1 LC connecting the mullion-to-spandrel beam web; (b) Test 2 LC connecting façade track-to-slab (refer to Figures 4a and 5a for LC locations).

In addition to the instrumentation above, high-speed video cameras were used at different viewing angles, outside and inside the structure, to capture the response of the building as loaded with the blast load. Finally, the building was surveyed before and after each test to assess any post-test damage and permanent lateral plastic deformation.

### 3.8. Test Procedure

Two blast tests were performed with the same explosive charge weight. The main difference between Test 1 and Test 2 was the façade enclosure of the steel frame. Test 1 was representative of a baseline case to evaluate the blast effects on a conventionally designed building that is enclosed with conventional, non-blast-resistant, curtainwall façade (Figure 4). For Test 2, the same steel frame was enclosed with a blast-resistant façade (Figure 5) in order to evaluate the effects of a non-failing façade on the steel frame and on the LFRS of a conventionally designed steel frame building with no provisions for resisting dynamic blast loads. For both tests, the explosive charge used was positioned on the south side and at the centerline of the structure, as shown in Figure 10. The standoff distance between the explosive charge and the structure was sufficiently large enough, resulting in an approximately uniform pressure on the reflected (south) elevation of the structure. Following completion of the first blast test, where the building was enclosed with the conventional glazed façade, described in Section 3.5, the damaged façade was removed and replaced with the blast-resistant steel façade described in Section 3.6, in preparation of the second blast test.

Since the structure was designed to represent a typical office building, the two elevated floors, i.e., second and third, were loaded with additional load, which is consistent with the load combination for extraordinary loading events ( $1.2 \times \text{dead} + 0.5 \times \text{live}$ ) per ASCE/SEI 7-10 [20]. This load combination represents the service loads on an operational building during an extraordinary event (fire, explosion, impact). For the design loads of the test structure, as outlined on Section 3.2 above, the required extra load, on top of the concrete slab self-weight, was  $3.0 \text{ kN/m}^2$ . The extra load on the test structure was approximated with nine (9), evenly spaced, concrete blocks per bay with dimensions  $0.9 \text{ m} \times 0.9 \text{ m} \times 0.65 \text{ m}$  (height). Each one of the two floors had five bays, resulting in a total of 90 concrete blocks total (45 blocks per floor). A view of the blocks after being placed in the structure is shown in Figure 11.

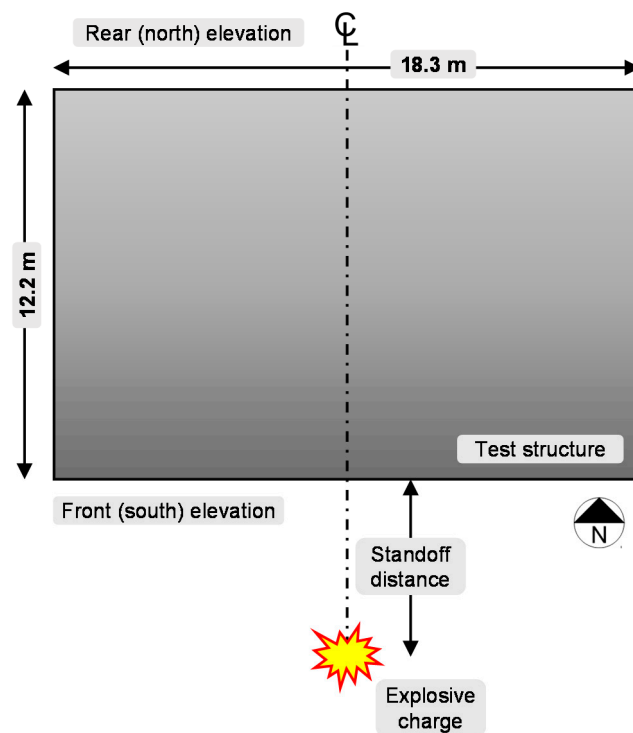


Figure 10. Overhead view of test configuration, which was the same for both tests.



Figure 11. View of the concrete blocks for approximating loads under operational conditions consistent with extraordinary load combination of ASCE/SEI 7-10 [20] (45 per floor, 90 total on 2nd & 3rd floors).

#### 4. Response of Test Structure to Blast Load

##### 4.1. Blast Test 1 on Frame with Conventional Façade

For the first test, the structure was enclosed with a conventional, non-blast-resistant, glazed curtainwall façade (Figure 4). Figure 12 shows a series of snapshots from highspeed video footage following the detonation of the explosive charge (Figure 12b) as the airblast shock wave propagated to the test structure. The airblast wave direction was from the south to the north (Figure 10) and first arrived on the south (front) elevation of the structure. The front face of the shock wave can be clearly seen on Figure 12c. Almost concurrently with the arrival of the shock wave, the first few glazed units shattered on the first floor, as indicated in Figure 12d. The glazing damage rapidly propagated to the entire front

elevation of the building, as shown in Figure 12e,f. Eventually, the exterior curtain wall façade failed almost instantaneously as the blast wave loaded the structure. Views of the post-test condition of the structure can be seen in Figure 13. Specifically, all front and rear elevation glazing completely shattered, and the aluminum mullions were severely damaged. Only a few glazed units remained intact at the side elevations of the building.

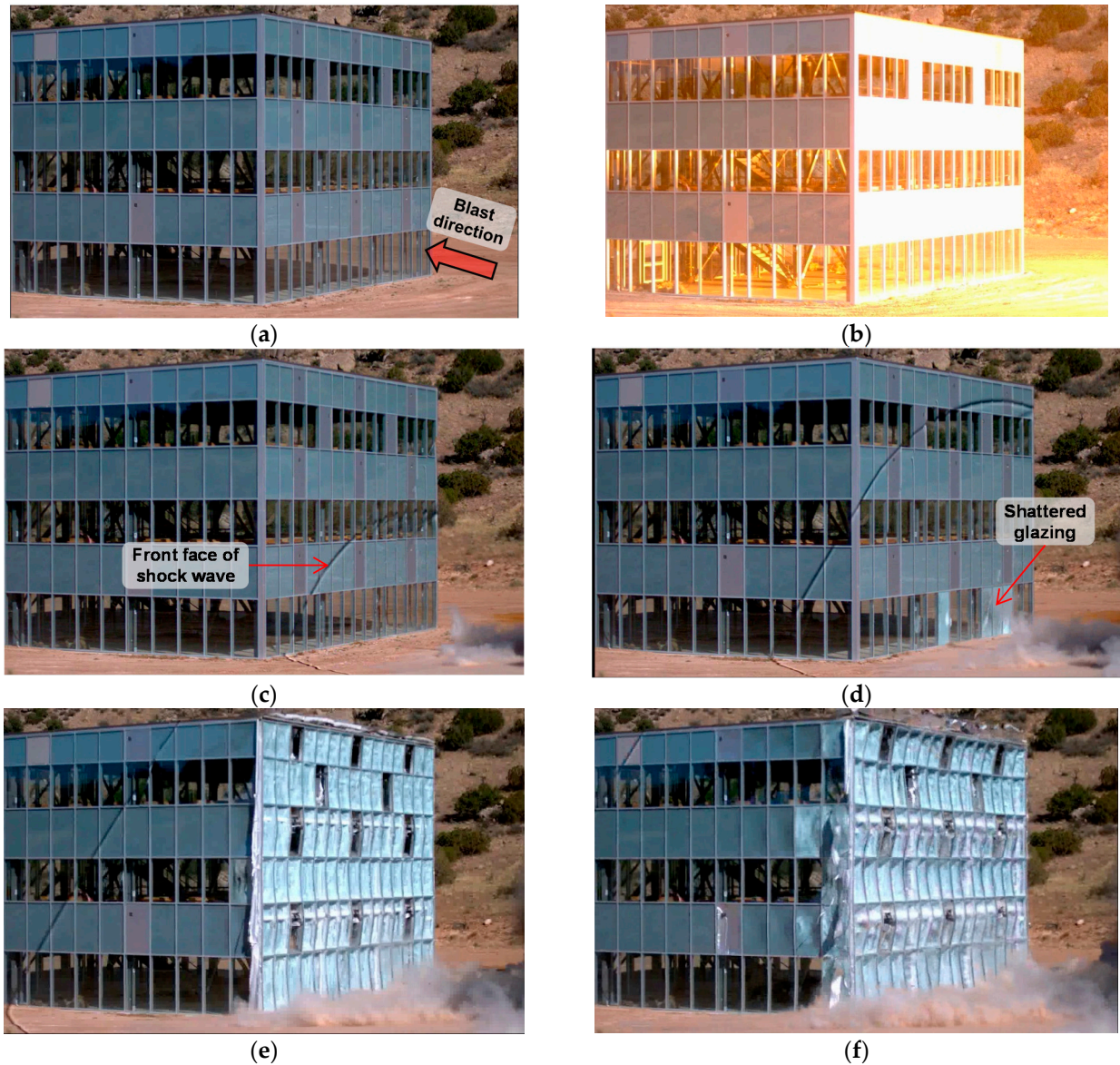


**Figure 12.** Test 1—Snapshots from high-speed video footage during test: (a) Prior to detonation; (b) Explosive charge detonation; (c) Arrival of shock wave; (d) Initial glazing failure on first floor; (e) Completely shattered glazing on front elevation; (f) Façade damage propagates to side façade.

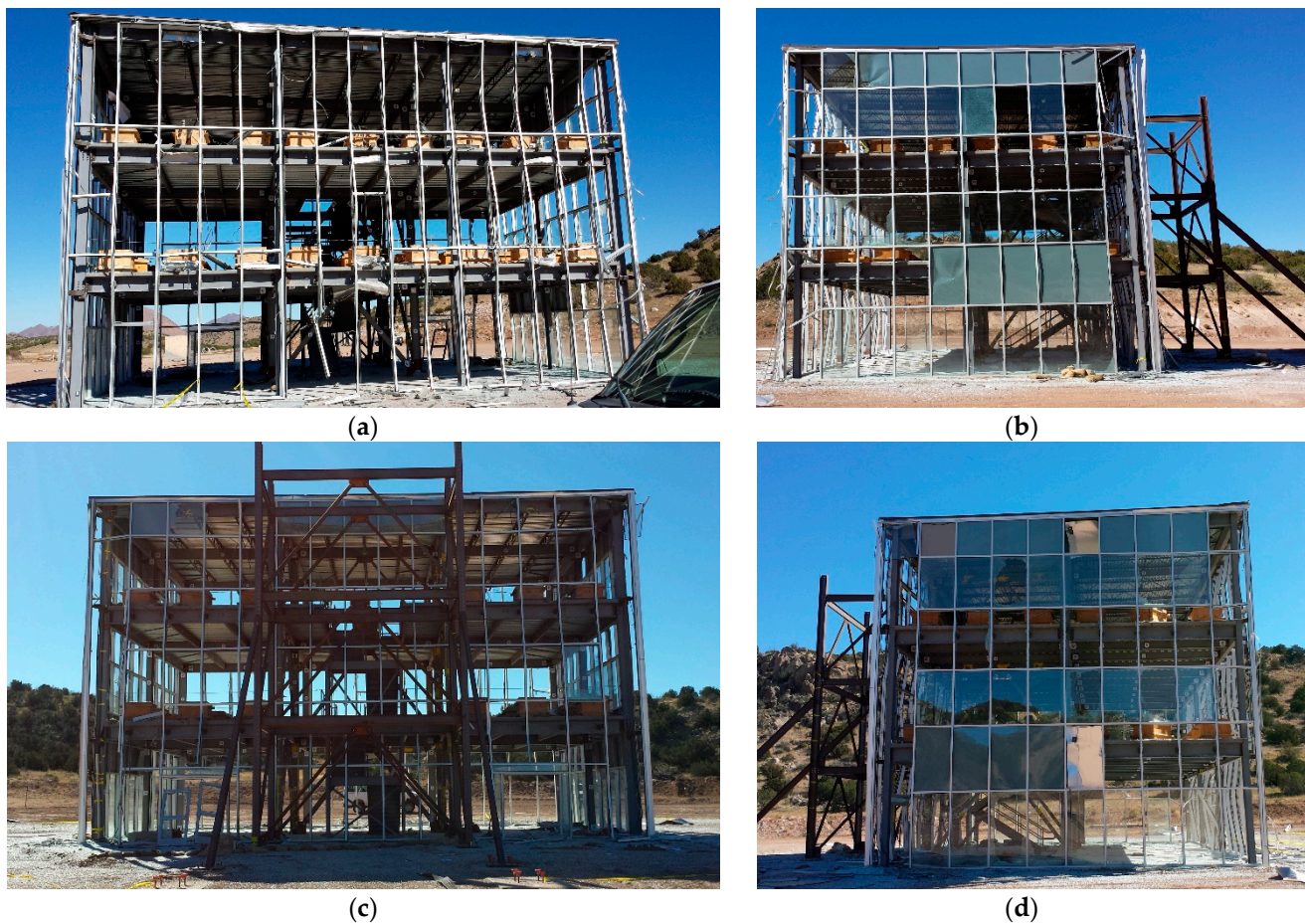


**Figure 13.** Test 1—Post-test condition of structure: (a) Front (south) elevation; (b) Side (east) elevation; (c) Rear (north) elevation; (d) Side (west) elevation.

The peak measured lateral deflections on the structure were recorded for the first inbound response cycle from the nine displacement gauges indicated in Figure 7, and these are summarized in Table 1. The measurements from the three sets of displacement gauges were relatively consistent. The peak lateral deflection of the roof was 33.0 mm. It was also observed that the peak deflection at all floor levels occurred almost concurrently, approximately 120 ms after the detonation. The peak deflection at the roof preceded the peak deflections of the lower floors by approximately 5–10 ms.

**Table 1.** Test 1—Measured peak inbound lateral deflection of the frame.

| Gauge Set | Gauge ID <sup>1</sup> | Floor | Peak Inbound Response <sup>2</sup> |                        |
|-----------|-----------------------|-------|------------------------------------|------------------------|
|           |                       |       | Deflection (mm)                    | Time <sup>3</sup> (ms) |
| 1         | DG1                   | 2nd   | 10                                 | 128                    |
|           | DG2                   | 3rd   | 23                                 | 121                    |
|           | DG3                   | roof  | 33                                 | 116                    |
| 2         | DG4                   | 2nd   | 15                                 | 141                    |
|           | DG5                   | 3rd   | 23                                 | 121                    |
|           | DG6                   | roof  | 33                                 | 115                    |
| 3         | DG7                   | 2nd   | 15                                 | 140                    |
|           | DG8                   | 3rd   | 20                                 | 141                    |
|           | DG9                   | roof  | 33                                 | 126                    |

<sup>1</sup> Refer to Figure 7 for locations of each gauge. <sup>2</sup> All peak deflections occurred at first inbound response cycle.

<sup>3</sup> Time after detonation.

The average deflections at each floor level from the three sets of displacement gauges are shown in Table 2 along with the estimated inter-story drift ratios, assuming the peak story deflections were concurrent. These inter-story drift ratios were approximately half of the 0.5% drift ratio of ASCE 41-06 [31] for performance level S-1 (Immediate Occupancy), which is described as “minor yielding or buckling of braces”. In fact, due to the rapid failure of the curtain wall façade, no damage was observed on the LFRS of the structure. All braces remained straight; i.e., no signs of buckling and none of the gusset plate connections of the braces (Figure 3c) ruptured. Essentially, the frame of the building responded elastically. As confirmed by survey data, there was no permanent lateral deformation on the structure. Despite the favorable response of the structural frame, the occupant survivability was expected to be quite low, since most of the glazed façade shattered and debris penetrated the building.

**Table 2.** Test 1—Average of peak inbound lateral deflections and estimated inter-story drift ratios.

| Floor Level        | Avg. Peak Inbound Deflection (mm) | Inter-Story Deflection (mm) | Inter-Story Drift Ratio <sup>1</sup> |
|--------------------|-----------------------------------|-----------------------------|--------------------------------------|
| roof               | 33                                | 11                          | 0.3%                                 |
| 3rd                | 22                                | 8                           | 0.2%                                 |
| 2nd                | 14                                | 14                          | 0.3%                                 |
| 1st (ground floor) | 0                                 | -                           | -                                    |

<sup>1</sup> Story height was 4.1 m.

The deflected shape of the structure at different stages between time of detonation (0 ms) up to the time of peak inbound response (120 ms) is shown in Figure 14a. In addition, Figure 14b shows the recorded deflection histories at each floor level, as measured from DG4, DG5, and DG6 for the 2nd, 3rd, and roof respectively. Following the peak inbound response, there was a free vibration stage after about 200 ms from which the fundamental period of the frame was estimated to be ≈380 ms.

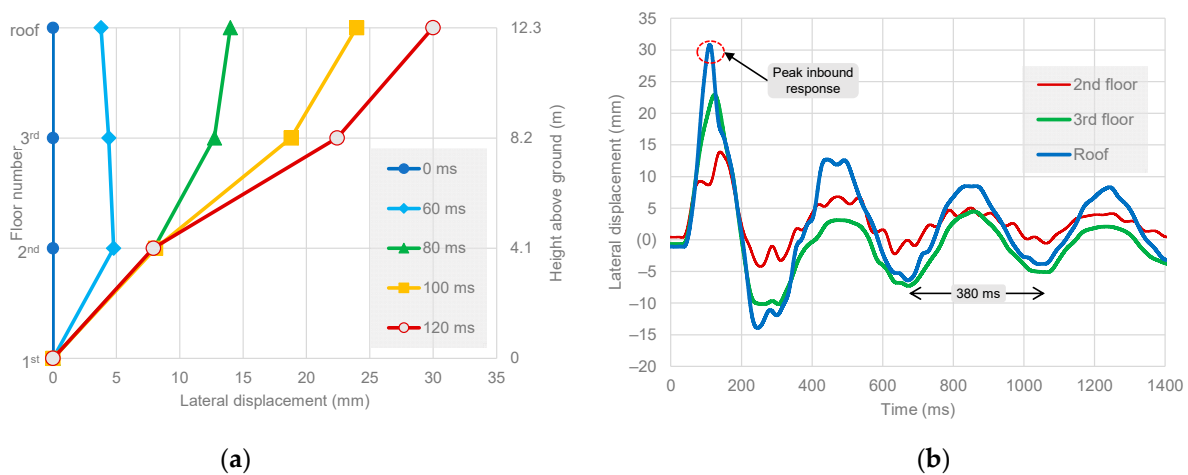


**Figure 14.** Test 1—Lateral response of structure: (a) Deflected shape at different times; (b) Lateral deflection history and estimation of natural period, data from DG4, DG5, and DG6.

The detonation of the explosive charge resulted in a peak-reflected specific impulse on the front (south) elevation (Figure 10) of the structure of 1350 kPa × ms. This impulse value was taken as the average value from the 11 PGs that were installed on the front elevation of the structure at various locations over the width and height. Considering the 18.3 m width and 12.3 m height of the building, the total impulse at the front elevation was 304 MN × ms. This relatively high impulse value was not transferred entirely to the LFRS of the structure, since the early, almost instantaneous, failure of the glazed façade (Figure 12c–f) reduced

considerably the “collected” blast load that was transferred to the mullions and eventually, through the mullion-to-spandrel beams connections (Figure 4c), to the steel frame. This observation was confirmed by the dynamic reaction histories measured from the two load cells connecting the mullion-to-spandrel beams (Figure 9a). Specifically, the load histories of the two load cells were integrated and divided by the tributary area of each connection point i.e., spacing of vertical mullions (1.2 m)  $\times$  floor height (4.1 m). The resulting value of  $\approx 120$  kPa  $\times$  ms provided an estimation of the peak specific impulse that the glazed façade transferred to the frame. This value was less than 10% of the 1350 kPa  $\times$  ms reflected specific impulse, as measured from the 11 PGs at the front of the structure.

Figure 8 shows the IDs of the 24 strain gauges that were attached to the braces of column lines B and C that were used to estimate the peak axial forces on the braces. Table 3 summarizes the peak measured brace forces. All peak forces were recorded during the first inbound response cycle; therefore, for each pair of chevron brace members, one value is negative, indicating compression, and the other value is positive due to tension. The brace forces progressively reduce from the first to the third floor. While there was some variation on brace loads between column lines B and C, overall, the peak measured loads were similar, indicating a nearly symmetric loading and response of the frame to the applied blast loads.

**Table 3.** Test 1—Peak measured braces forces from strain gauge data (refer to Figure 8 for strain gauge positions).

| Floor | Gauge ID <sup>1</sup> | Brace Member Size             | Brace Cross-Sectional Area (mm <sup>2</sup> ) | Braces along Column Line B            |  | Braces along Column Line C            |  |
|-------|-----------------------|-------------------------------|---|---------------------------------------|--|---------------------------------------|--|
|       |                       |                               |   | Measured Peak Force <sup>2</sup> (kN) | Estimated Peak Force per Brace <sup>3</sup> (kN) | Measured Peak Force <sup>2</sup> (kN) | Estimated Peak Force per Brace <sup>3</sup> (kN) |
| 1st   | SG1 (SG13)            | HSS6 $\times$ 6 $\times$ 3/16 | 2568  | −377                                  | −402   | −676                                  | −545   |
|       | SG2 (SG14)            |                               | 2568  | −426                                  |  | −415                                  |  |
|       | SG3 (SG15)            | HSS6 $\times$ 6 $\times$ 3/16 | 2568  | 460                                   | 459  | 462                                   | 479  |
|       | SG4 (SG16)            |                               | 2568  | 457                                   |  | 496                                   |  |
| 2nd   | SG5 (SG17)            | HSS5 $\times$ 5 $\times$ 3/16 | 2116  | −395                                  | −426   | −465                                  | −443   |
|       | SG6 (SG18)            |                               | 2116  | −457                                  |  | −420                                  |  |
|       | SG7 (SG19)            | HSS5 $\times$ 5 $\times$ 3/16 | 2116  | 421                                   | 423  | 409                                   | 413  |
|       | SG8 (SG20)            |                               | 2116  | 424                                   |  | 416                                   |  |
| 3rd   | SG9 (SG21)            | HSS4 $\times$ 4 $\times$ 3/16 | 1665  | −216                                  | −215   | −122                                  | −164   |
|       | SG10 (SG22)           |                               | 1665  | −215                                  |  | −206                                  |  |
|       | SG11 (SG23)           | HSS4 $\times$ 4 $\times$ 3/16 | 1665  | 172                                   | 178  | 183                                   | 173  |
|       | SG12 (SG24)           |                               | 1665  | 184                                   |  | 164                                   |  |

<sup>1</sup> IDs within brackets are strain gauges on column line C braces. <sup>2</sup> Taken at the peak measured strain multiplied by steel elastic modulus (200 GPa) and by brace cross-sectional area. <sup>3</sup> Taken as the average of the measured peak force from the two strain gauges at each brace member.

#### 4.2. Blast Test 2 on Frame with Blast-Resistant Façade

Following the completion of the first blast test, the damaged glazed façade was removed and replaced with the steel, blast-resistant façade (Figure 5). Figure 15 shows a series of snapshots from high-speed video footage following the detonation as the pressure wave propagated through the structure. The explosive charge weight and position were the same as for the first test (Figure 10). Figure 15c,d indicate the propagation of the front face of the pressure wave on the structure. A few milliseconds later, the front façade started responding to the applied load, as shown in Figure 15e. At this stage, the façade was still loaded with the inbound positive pressure from the airblast, which is reflected on the deformed shape of the corrugated deck siding on the second and third floors. The first-floor siding, which was comprised of a 16 mm thick steel plate (Figure 5a), remained practically elastic with minimal inbound deformation. As the pressure wave propagated, the negative phase of the airblast wave arrived, which is reflected in Figure 15f where some of the corrugated deck siding started to detach from the supporting channel members (Figure 5b).

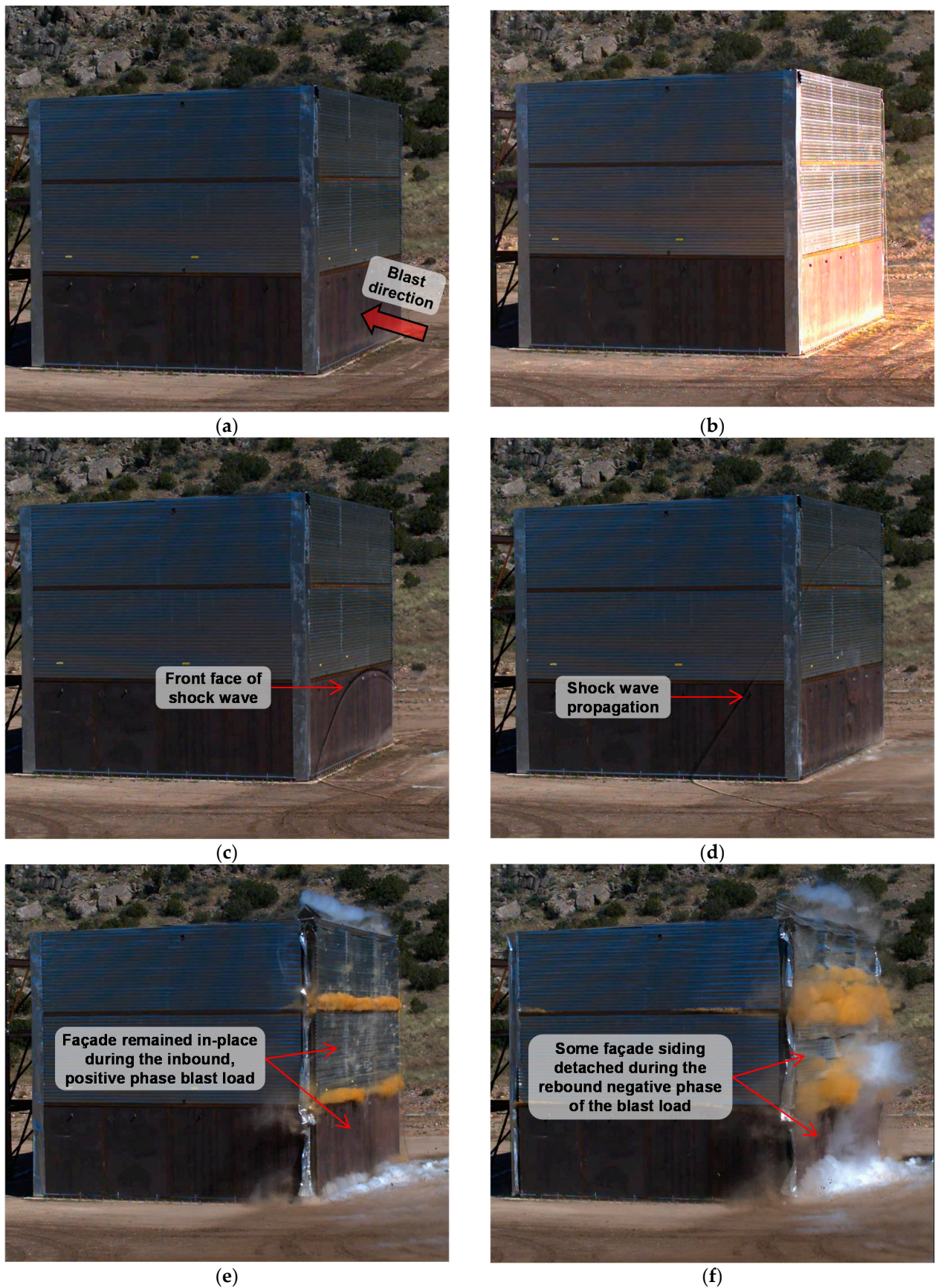


**Figure 15.** Test 2—Snapshots from high-speed video footage during test: (a) Prior to detonation; (b) Explosive charge detonation; (c) Arrival of shock wave; (d) Propagation of shock wave over the structure; (e) Inbound loading of the front face facade; (f) Rebound response of the front face facade.

Figure 16 shows the condition of the structure after the test. As shown in Figure 16a, most of the corrugated siding was detached due to the negative phase of the airblast load. Based on visual inspection, the vertical façade members at the second and third floors responded within the expected response limits. As previously noted in Section 3.6, the performance limit was a peak lateral deformation 215 mm or less. In fact, in Figure 16b, the residual plastic deformation of the façade channels was approximately 150 mm.

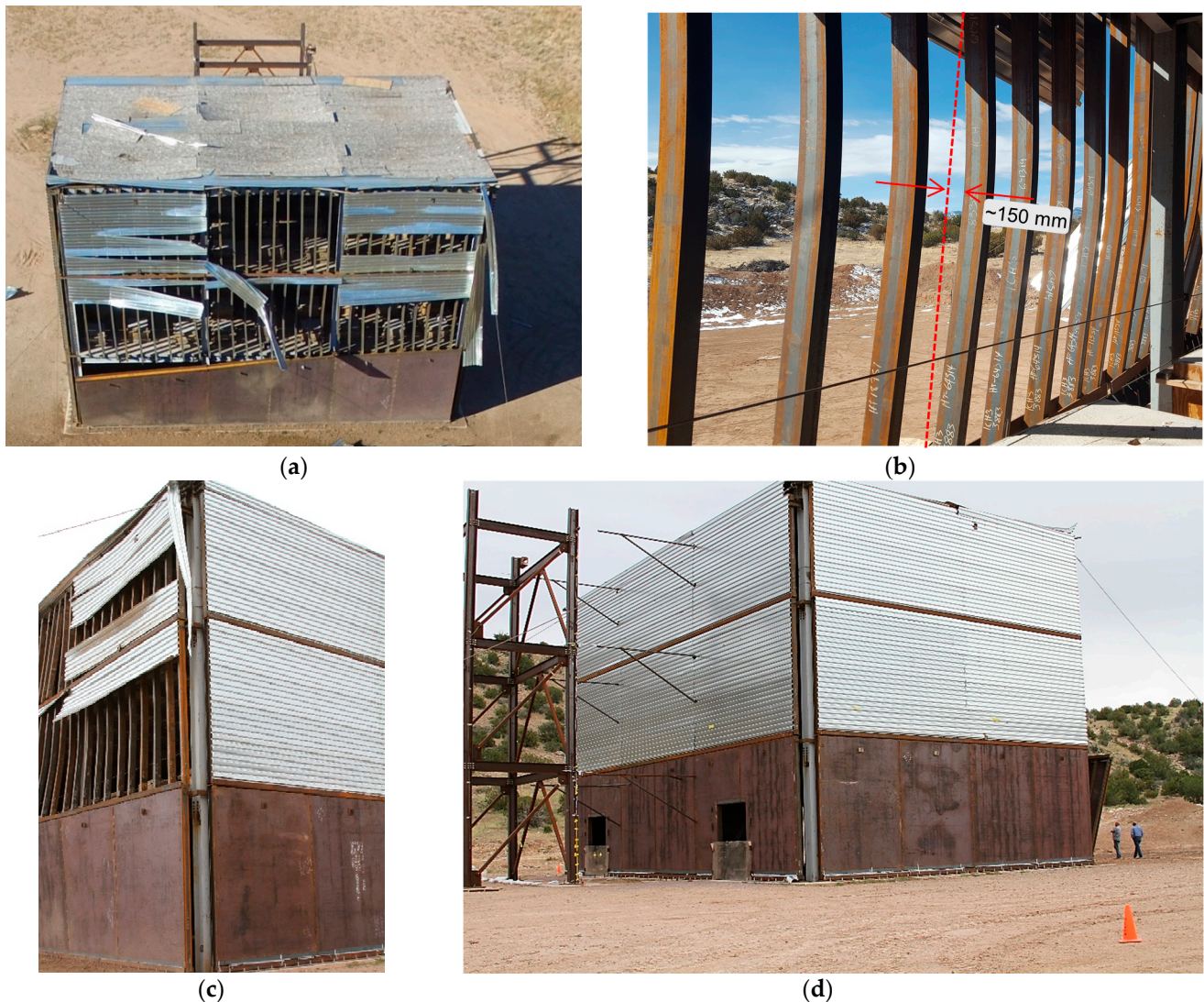


**Figure 16.** Test 2—Post-test condition of structure: (a) Aerial view of front (south) elevation; (b) View from 2nd floor (looking southwest); (c) Southeast elevation; (d) Northwest elevation.

Most of the façade connections at the second-floor level failed where the façade channels slipped out of the track during the rebound (Figure 5c). The connections at this level failed due to the higher dynamic reactions caused by the composite action of the 16 mm thick steel plate that was welded to the first-floor vertical façade channels (Figure 5b). Specifically, some bolts that connected the vertical channels to the frame ruptured in direct shear during the inbound response. During the negative phase of the airblast, the façade ends were not positively connected to the structure anymore, causing a zipper-type failure mode with the façade detaching from the frame. This connection failure did not affect the inbound blast load that was transferred to the steel frame. During the inbound response and as bolts ruptured, the façade channels transferred the blast load to the structure through direct bearing action with the edge of the concrete slab, since the

gap between the slab edge to the façade channels was less than 50 mm, as can be seen in Figure 9b.

In general, the peak lateral deflections of the frame were higher compared to the first test (Table 1). Table 4 shows the peak measured lateral deflections during the first inbound response cycle, as measured from the displacement gauges shown in Figure 7. At the roof level, the peak deflection of  $\approx 85$  mm occurred first, which was approximately 120 ms after the detonation, and after about 40–50 ms, the second and first floor also reached their peak displacement.

**Table 4.** Test 2—Measured peak inbound lateral deflection of the frame.

| Gauge Set | Gauge ID <sup>1</sup> | Floor | Peak Inbound Response <sup>2</sup> |                        |
|-----------|-----------------------|-------|------------------------------------|------------------------|
|           |                       |       | Deflection (mm)                    | Time <sup>3</sup> (ms) |
| 1         | DG1                   | 2nd   | 56                                 | 174                    |
|           | DG2                   | 3rd   | 74                                 | 140                    |
|           | DG3                   | roof  | 79                                 | 123                    |
| 2         | DG4                   | 2nd   | 58                                 | 186                    |
|           | DG5                   | 3rd   | 84                                 | 143                    |
|           | DG6                   | roof  | 86                                 | 123                    |
| 3         | DG7                   | 2nd   | 58                                 | 163                    |
|           | DG8                   | 3rd   | 81                                 | 143                    |
|           | DG9                   | roof  | 89                                 | 123                    |

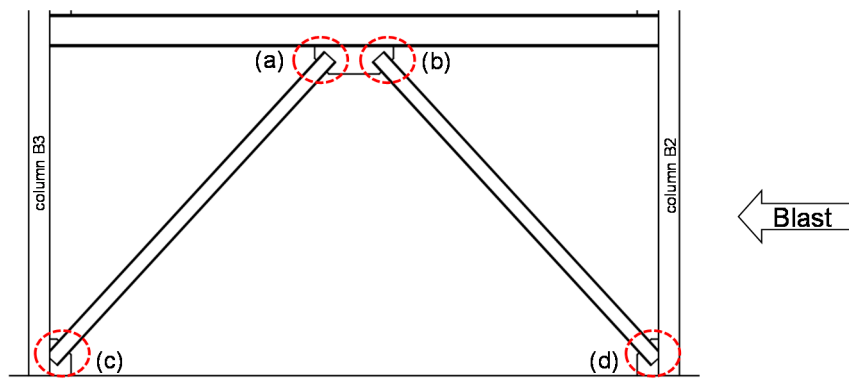
<sup>1</sup> Refer to Figure 7 for locations of each gauge. <sup>2</sup> All peak deflections occurred at first inbound response cycle. <sup>3</sup> Time after detonation.

The average recorded deflections are shown in Table 5, which are taken as the average of the floor deflections from the three sets of displacement gauges (Table 4). This table also shows the estimated inter-story drift ratios, assuming the peak story deflections occurred concurrently. Specifically, the second-floor inter-story drift was 1.4%, which is only 0.1% lower than the 1.5% drift ratio limit of ASCE 41-06 [31] for performance level S-3 (Life Safety) “*many braces yield or buckle but do not totally fail. Many connections may fail*”. In fact, as shown in Figures 17d and 18c, two gusset plate brace connections on the first floor of the two braces that were in tension during the inbound response (direction of applied blast load) completely ruptured. Additionally, the connections of the conjugate first-floor braces that were in compression during the inbound response yielded and had some signs of fracture initiation at the weld lines, as indicated in Figures 17c and 18b. A magnified view of the gusset plate joint of Figure 18b can be seen in Figure 19 where the yielding and rupture initiation are apparent. On the second and third floors where the story drift ratios were 0.5% and 0.2%, respectively, which were equal or less to the drift ratio limit for performance level S-1 (Immediate Occupancy) per ASCE 41-06 [31], there was no apparent damage to the braces and their gusset plate connections. Despite the partial damage to the first-floor brace connections, it was verified by survey data that the permanent lateral deformation on the structure was less than 3 mm at the roof level. Globally, the frame did not have signs that it was at the near-collapse state. However, the building was not considered safe for immediate occupancy until after the damaged LFRS was repaired.

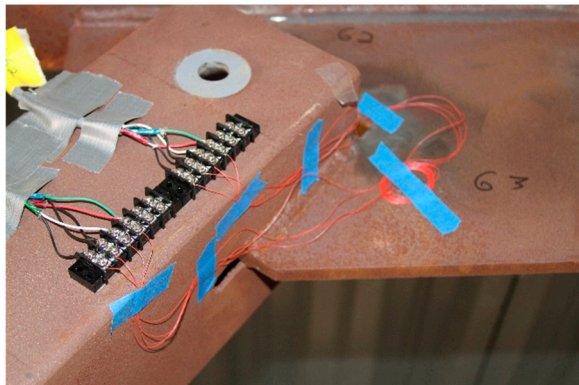
**Table 5.** Test 2—Average of peak inbound lateral deflections and estimated inter-story drift ratios.

| Floor Level        | Avg. Peak Inbound Deflection (mm) | Inter-Story Deflection (mm) | Inter-Story Drift Ratio <sup>1</sup> |
|--------------------|-----------------------------------|-----------------------------|--------------------------------------|
| roof               | 86                                | 7                           | 0.2%                                 |
| 3rd                | 79                                | 21                          | 0.5%                                 |
| 2nd                | 58                                | 58                          | 1.4%                                 |
| 1st (ground floor) | 0                                 | -                           | -                                    |

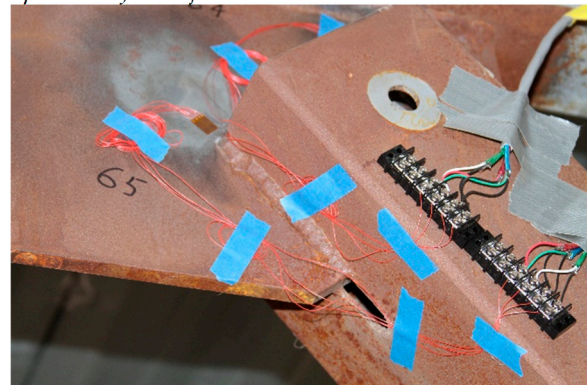
<sup>1</sup> Story height was 4.1 m.



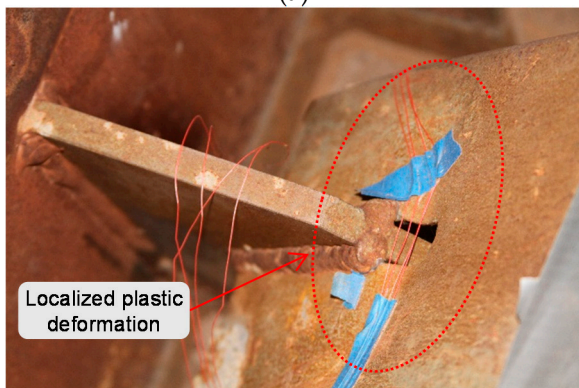
red circles indicate the close-up views of each joint



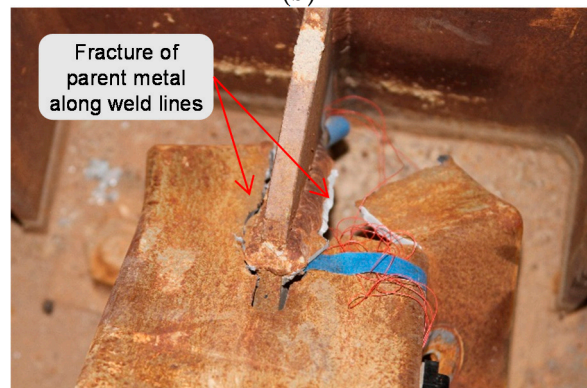
(a)



(b)



(c)



(d)

**Figure 17.** Test 2—First floor brace connections at column line B: (a) Top gusset joint closer to column B3; (b) Top gusset joint closer to column B2; (c) Base gusset joint with column B3; (d) Base gusset joint with column B2.

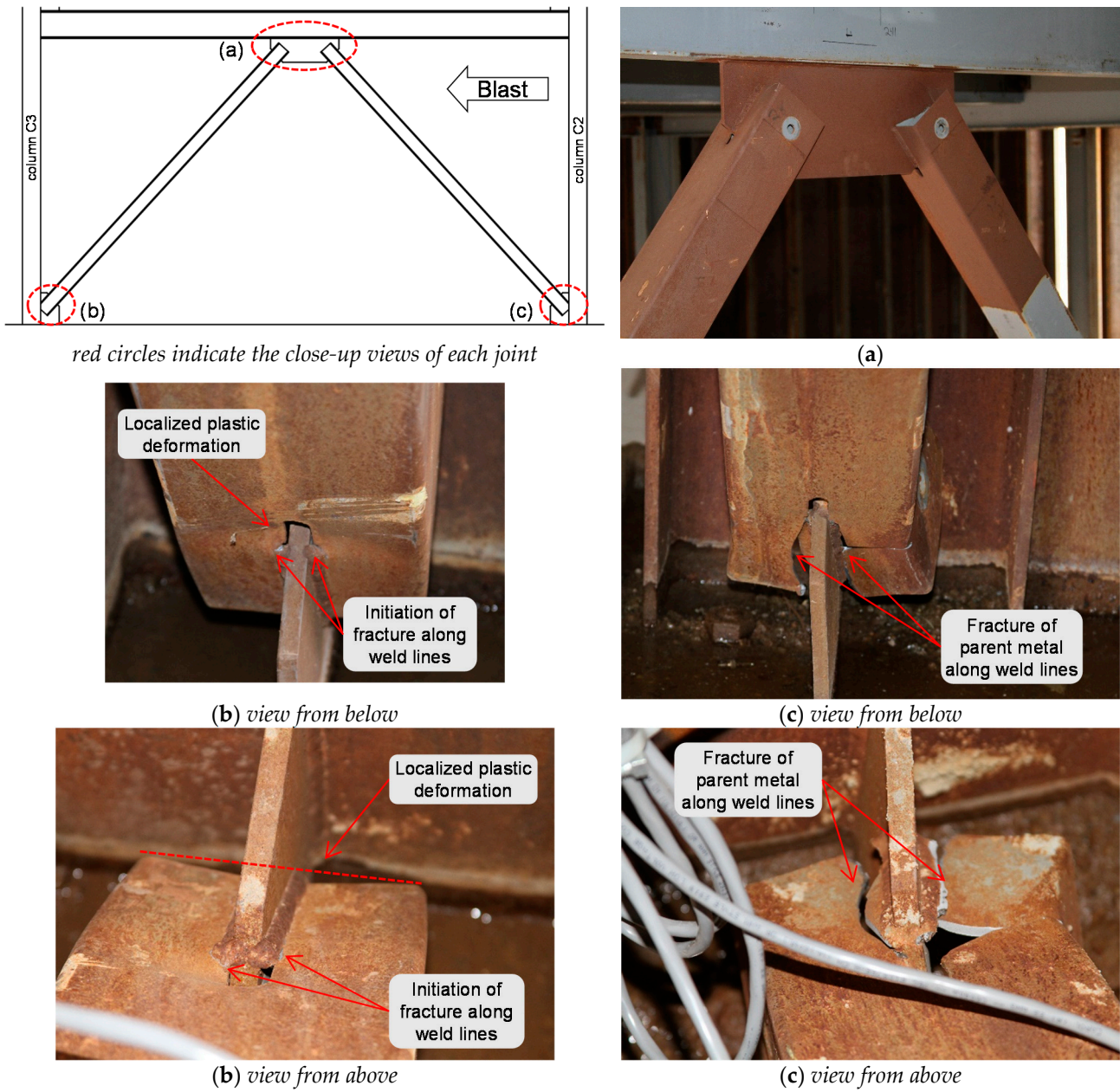


**Figure 18.** Test 2—First floor brace connections at column line C: (a) Top gusset joints; (b) Base gusset joint with column C3 (see Figure 19 for a magnified view); (c) Base gusset joint with column C2.

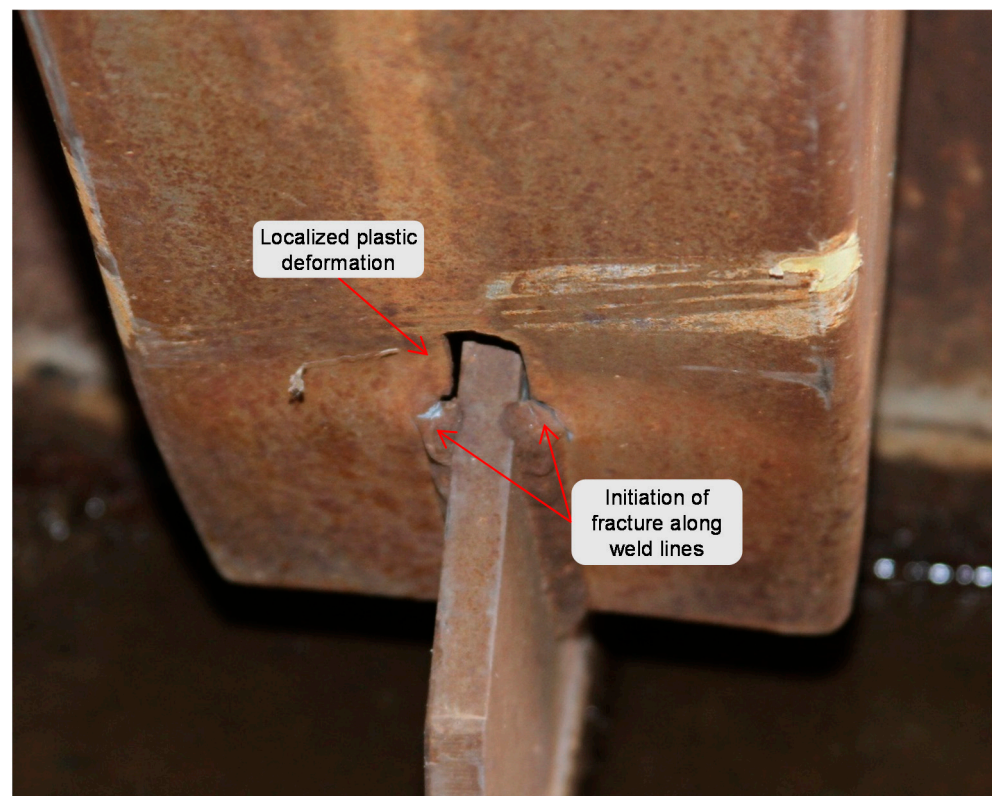


**Figure 19.** Magnified view of Figure 18b.

The deflected shape of the structure at different stages between the time of detonation (0 ms) and a few milliseconds past the peak inbound response (120 ms) is shown in Figure 20a. Figure 20b shows the lateral deflection histories at the three floor levels as recorded by DG4, DG5, and DG6 for the 2nd, 3rd, and roof, respectively. The natural period of the frame was estimated to be approximately 820 ms, which was more than twice as high as the estimated natural period of the frame during the first test that was  $\approx 380$  ms. The rupture of the two first-floor brace connections (Figures 17d and 18c) were the primary reason for the higher natural period. Basically, two out of the four brace members on the first floor were not participating in the LFRS; hence, the lateral stiffness of the frame dropped, which resulted in an increase in the natural period. A secondary reason for the increase in the natural period was due to the overall increase in the building mass due to the heavier blast-resistant façade (Figure 5) that the frame had during this test compared to the lighter conventional façade used for the first test (Figure 4).

As mentioned earlier, to eliminate the participation of the relatively strong façade in the resisting lateral load, the base connection of the curtainwall façade at each floor level was designed to move along (slide) with the floor above (Figure 5c). Footage from high-speed video cameras that were focused on the base connections of the curtainwall façade at the west side of the building were reviewed, and it was confirmed that the façade was moving along with the floors. Figure 21 shows the motion relative to the base channel lateral displacement of the first-floor curtainwall façade at the west side of the building. The relative motion at 125 ms was estimated to be  $\approx 50$  mm, which was in phase with the measured displacement of the second floor at the same time (Figure 20a).

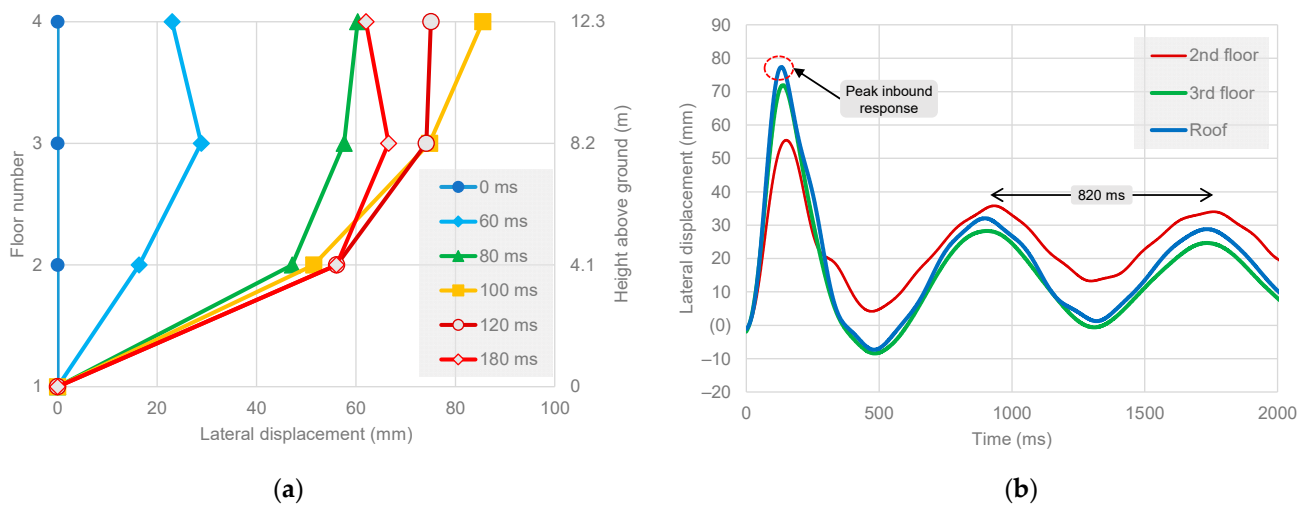


**Figure 20.** Test 2—Lateral response of structure: (a) Deflected shape at different times; (b) Lateral deflection history and estimation of natural period, data from DG4, DG5, and DG6.

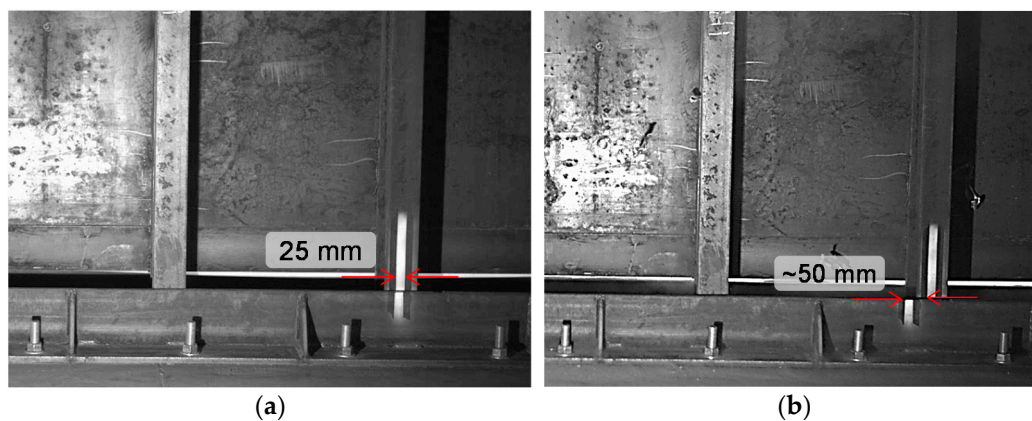


**Figure 21.** Test 2—Close-up views of the base sliding connection (south to north direction) of the first-floor curtainwall façade at the west elevation of the building (high-speed camera inside the building looking west): (a) Time = 0 ms; (b) Time = 125 ms after detonation.

The peak-reflected specific impulse on the front (south) face of the building (Figure 10) was  $1500 \text{ kPa} \times \text{ms}$ , which was approximately 10% higher than the impulse during the first test. As with the first test, the impulse value was taken as the average from the 11 PGs that were installed on the front elevation of the building. Multiplying this value with the front face dimensions of the building, 18.3 m wide and 12.3 m tall, the reflected impulse was  $350 \text{ MN} \times \text{ms}$ . Unlike the conventional glazed façade during the first test, the blast-resistant façade absorbed most of the blast impulse that was eventually transferred to the LFRS of the building. Unfortunately, the loads cells that were installed to measure the dynamic reactions that the façade transferred to the frame (Figure 9b) were damaged during the test, and the recorded data were not valid. Nonetheless, the higher impulse that the nonfailing façade transferred to the building frame, compared to Test 1, was evident from the generally higher lateral deflections and the partial failure of the first-floor brace connections (Figures 17 and 18). Additionally, the higher impulse that was transferred to the building was also reflected on the response of roof spandrel beams on the front (south) elevation of the building, as shown in Figure 22. The roof spandrel beams had an appreciable level of permanent lateral deformation i.e., weak axis bending, of approximately 300 mm. Conversely, the same spandrel beams after the first test did not have any permanent deformation. Since the spandrels at the lower floors were connected

to the concrete slab through shear studs, their weak axis bending capacity was higher; hence, they did not sustain any plastic deformation about their weak axis.



Figure 22. Test 2—View from 3rd floor looking at the bent spandrel beams of roof.

Finally, Table 6 shows the peak measured brace forces based on the recorded data from the 24 strain gauges that were attached to each one of the 12 braces that resisted load in the blast direction (Figure 8). The peak forces for all braces were recorded during the first inbound response cycle. Consequently, for each pair of braces, the negative value is at the brace member in compression and the positive value is for the conjugate brace that was in tension. It is also noted that the base connections of SG3, SG4, SG15, and SG16 that were attached to the brace members completely ruptured (Figures 17d and 18c).

Table 6. Test 2—Peak measured braces forces from strain gauge data (refer to Figure 8 for strain gauge positions).

| Floor | Gauge ID <sup>1</sup> | Brace Member Size | Brace Cross-Sectional Area (mm <sup>2</sup> ) | Braces along Column Line B            |  | Braces along Column Line C            |  |
|-------|-----------------------|-------------------|---|---------------------------------------|--|---------------------------------------|--|
|       |                       |                   |   | Measured Peak Force <sup>2</sup> (kN) | Estimated Peak Force per Brace <sup>3</sup> (kN) | Measured Peak Force <sup>2</sup> (kN) | Estimated Peak Force per Brace <sup>3</sup> (kN) |
| 1st   | SG1 (SG13)            | HSS6 × 6 × 3/16   | 2568  | -1241                                 | -974   | -654                                  | -681   |
|       | SG2 (SG14)            |                   | 2568  | -707                                  |  | -707                                  |  |
|       | SG3 (SG15)            | HSS6 × 6 × 3/16   | 2568  | <u>814</u>                            | <u>796</u>                                       | <u>841</u>                            | <u>827</u>                                       |
|       | SG4 (SG16)            |                   | 2568  | <u>778</u>                            |  | <u>814</u>                            |  |
| 2nd   | SG5 (SG17)            | HSS5 × 5 × 3/16   | 2116  | -498                                  | -514   | ×                                     | -730   |
|       | SG6 (SG18)            |                   | 2116  | -529                                  |  | -730                                  |  |
|       | SG7 (SG19)            | HSS5 × 5 × 3/16   | 2116  | 507                                   | 465  | ×                                     | n/a  |
|       | SG8 (SG20)            |                   | 2116  | 423                                   |  | ×                                     |  |
| 3rd   | SG9 (SG21)            | HSS4 × 4 × 3/16   | 1665  | -280                                  | -294   | ×                                     | -347   |
|       | SG10 (SG22)           |                   | 1665  | -307                                  |  | -347                                  |  |
|       | SG11 (SG23)           | HSS4 × 4 × 3/16   | 1665  | 245                                   | 249  | 503                                   | 405  |
|       | SG12 (SG24)           |                   | 1665  | 254                                   |  | 307                                   |  |

<sup>1</sup> IDs within brackets are strain gauges on column line C braces. <sup>2</sup> Taken at the peak measured strain multiplied by steel elastic modulus (200 GPa) and by brace cross-sectional area. <sup>3</sup> Taken as the average of the measured peak force from the two strain gauges at each brace member. Underlined values are on the braces that their connections ruptured. '×' indicates strain gauge data were not good.

#### 4.3. Test 1 and Test 2 Response Comparison and Remarks

Even though the applied blast impulse in the two tests was practically the same, in the order of 1350–1500 kPa × ms, the responses were significantly different. Since the only difference on the test structure between Test 1 and Test 2 was the envelope of the building,

it is quite evident that the presence of the hardened (blast-resistant) façade during Test 2 collected and transferred a significantly higher dynamic lateral load to the structural frame of a building compared to Test 1 where the conventional glazed façade failed early, thus transferring less load to the frame. Table 7 summarizes the peak inbound lateral deflections from the two tests. The peak measured deflections during the second test were more than 2.5 times higher compared to the lateral deflections of the first test, which indicates the considerably higher blast impulse that the building frame absorbed during the second test. In particular, at the second floor level, the difference was actually more than four times higher, since the rupture of the gusset plate brace connections of the first-floor braces (Figures 17 and 18) further increased the lateral displacements.

**Table 7.** Comparison of average of peak inbound lateral deflections for Test 1 and Test 2.

| Floor <sup>1</sup> | Avg. Peak Inbound Deflection (mm) |                               | Difference |
|--------------------|-----------------------------------|-------------------------------|------------|
|                    | Test 1—Conventional Glazed Façade | Test 2—Blast-Resistant Façade |            |
| roof               | 33                                | 86                            | 260%       |
| 3rd                | 22                                | 79                            | 360%       |
| 2nd                | 14                                | 58                            | 415%       |

<sup>1</sup> Story height was 4.1 m.

The higher loads that the LFRS resisted during the second test were also reflected on the estimated peak brace axial loads as recorded by the array of strain gauges (Figure 8). Table 8 shows a side-by-side comparison of the peak measured brace forces between the two tests. The brace forces during the second test were up to 2.4 times higher than those of the first test. In addition, as previously noted, the LFRS during the first test responded within the elastic regime with no signs of failure, whereas during the second test, the LFRS was partially compromised. Specifically, the gusset plate connections of the first-floor braces were either partially damaged due to local yielding (Figure 19) or completely ruptured along the weld lines d and Figure 18c). The partial damage of the first-floor brace connections acted as a “fuse-link” that limited the peak forces on the LFRS members. If the brace connections had higher capacity, it is likely that the braces forces would have been higher. Nonetheless, despite the partially compromised LFRS after the second test, the building remained practically vertical with less than 3 mm permanent lateral deformation at the roof level as measured from survey scans before and after the test.

**Table 8.** Test 1—Peak measured braces forces from strain gauge data (refer to Figure 8 for strain gauge positions).

| Floor | Brace Member Size | Estimated Peak Force per Brace <sup>1</sup> (kN) |            |            |                            |              |            |
|-------|-------------------|--|------------|------------|----------------------------|--------------|------------|
|       |                   | Braces along Column Line B                       |            |            | Braces along Column Line C |              |            |
|       |                   | Test 1   | Test 2     | Difference | Test 1                     | Test 2       | Difference |
| 1st   | HSS6 × 6 × 3/16   | −402   | −974       | 240%       | −545                       | −681         | 125%       |
|       | HSS6 × 6 × 3/16   | 459  | <u>796</u> | 175%       | 479                        | <u>827</u>   | 175%       |
| 2nd   | HSS5 × 5 × 3/16   | −426   | −514       | 120%       | −443                       | −730         | 165%       |
|       | HSS5 × 5 × 3/16   | 423  | 465        | 110%       | 413                        | no good data | —          |
| 3rd   | HSS4 × 4 × /3/16  | −215   | −294       | 140%       | −164                       | −347         | 210%       |
|       | HSS4 × 4 × /3/16  | 178  | 249        | 140%       | 173                        | 405          | 235%       |

<sup>1</sup> Taken as the average of the measured peak force from the two strain gauges at each brace member. Underlined values are on the braces that their connections ruptured.

In terms of occupant survivability, it should be highlighted that the shattered façade during the first test would have likely result in casualties due to the high-velocity debris from the shattered glazed façade. The debris would have likely injured the building’s occupants and casualties may have occurred, despite the essentially elastic response of the building’s frame. On the other hand, during the second test, even though the LFRS was

partially compromised, and peak lateral deflections were higher, occupant survivability was expected to be quite high since the hardened façade protected the interior of the building. Nonetheless, the building after the second test was not to be occupied immediately until after the damaged LFRS was repaired.

## 5. Research Limitations

While the full-scale test structure used for this test program constitutes in many ways a worst-case scenario, it may still not be representative for all steel frame building sizes and configurations. This test structure is considered to represent a worst-case scenario for the following reasons:

- It was designed to resist only typical gravity load and wind loads for a basic wind speed of 51 m/s.
- No provisions for blast or earthquake loads were considered.
- The chevron brace configuration used for the LFRS was found to be one of the most vulnerable brace types under dynamic overload conditions, as suggested by McKay et al. [19].
- The size and number of stories of the structure were also chosen based on the findings of the study by McKay et al. [19]. In similar blast environments, larger structures with more stories are likely to perform better. Conversely, smaller structures with a smaller number of stories are expected to have heavy damage and are prone to total collapse.
- The structure was oriented relative to the applied blast load such that the wider, 18.3 m, face of the building (Figure 10) was the one directly loaded from the airblast, which resulted to higher blast impulse loads compared to having the airblast directly loading the narrower, 12.2 m, face of the building.

More vulnerable steel building configurations/shapes may exist. For example, building geometries with concave shapes or re-entrant corners tend to “collect” more blast loads [1]; hence, their response to blast load is expected to be worse compared to a similar buildings with flat planar faces, which is similar to the one used for the tests herein. Secondly, while the blast load levels that the building was subjected to during the tests were relatively high, in the order of  $1500 \text{ kPa} \times \text{ms}$ , there is no assurance that if the same building was subjected to even higher blast load levels that it would not collapse. Nonetheless, the results from these series of blast tests on the three-story test structure provided valuable data about the response of steel structures for dynamic load ranges that exceed their design loads per structural code provisions of standard practice [20,21,29]. These tests demonstrated that steel buildings with three stories or more have the potential to withstand relatively high blast loads that can globally sway the structural frame of the building with a relatively high margin of safety against collapse to allow evacuation after an attack. However, the building was not considered to be suitable for immediate occupancy until after its LFRS was fully repaired. Finally, the experimental data from these tests will help improve structural analysis methods, as they can be used to validate existing approaches for assessing the response of structures under shock loads.

## 6. Summary and Conclusions

This paper presents the results of two large-scale blast tests that were conducted to evaluate the response of conventionally designed three-story steel frame buildings to relatively high, long duration blast loads. The LFRS of the test frame was designed only for typical gravity and wind loads without consideration for blast and/or seismic loads. The two tests were performed on the same steel frame and at the same blast load level. The only difference between the two tests was the envelope of the building. For the first test, the frame was enclosed with a conventional curtainwall glazed façade, while for the second blast test, the building was enclosed with a hardened blast-resistant façade. During the first test, the glazed façade failed early with minimal absorption of the applied blast impulse, and the steel frame responded elastically to the applied blast load. The LFRS was inspected after the test, and no damage was observed. Conversely, during the second

test, the non-failing hardened façade absorbed a higher level of blast load, which was transferred to the LFRS of the test structure, resulting in partial damage of some gusset plate connections at the first-floor level. Despite the partial damage of the LFRS, the steel frame resisted the applied blast load and provided a relatively high margin of safety against collapse since the post-test permanent lateral deflection at the roof level was estimated to be less than 3 mm. The response of the two tests and observations made during the test lead to the following remarks and conclusions:

- During the first test, the early failure of the conventional façade limited the blast loads that were transferred to the building; hence, no signs of damage or failure were observed on the LFRS of the test frame. Nonetheless, the occupant survivability in that case was expected to be quite low, since most of the glazed façade shattered and debris penetrated the building.
- Due to the early failure of the glazed façade during the first test, the estimated reflected impulse that the non-blast-resistant glazed façade transferred to the structural frame of the building was estimated to be only 10% of the measured reflected impulse at the front face of the building.
- During the second test, the blast-resistant façade sustained the inbound blast pressure with plastic deformation that was within the target performance limit, thereby transferring a considerably higher load to the LFRS of the test frame.
- Owing to the higher dynamic reactions during the second test, the LFRS was partially compromised with some gusset plate connections of the braces completely rupturing.
- The inter-story drift ratios of both tests were compared with the drift ratio limits of ASCE 41-06 [31] for the different performance levels. The agreement between the code-based drift ratio limit and the expected level of damage was consistent with the damage levels observed in the two tests.
- Despite the partial compromise of the LFRS during the second test, the building did not show any signs that it was at a near-collapse state, indicating that the safety margin against collapse was relatively high and would allow evacuation after an attack. Pre- and post-test survey data suggested that the steel frame only had a residual permanent plastic deformation at the roof level of approximately 3 mm.
- Due to the partial damage of the LFRS during the second test, the building was not considered suitable for immediate occupancy until after its LFRS was fully repaired.
- While the building used for the test program was considered a worst-case scenario since its LFRS was designed for typical winds load only without any provisions for blast or seismic loads, other building configurations with concave shapes of similar size may exist that may have a less favorable response.

**Author Contributions:** Conceptualization, M.H., A.E.M. and P.C.B.; methodology, M.H. and A.E.M.; software, M.H. and A.E.M.; validation, M.H., A.E.M. and P.C.B.; formal analysis, M.H. and A.E.M.; investigation, M.H., A.E.M. and P.C.B.; resources, A.E.M. and P.C.B.; data curation, M.H. and A.E.M.; writing—original draft preparation M.H.; writing—review and editing, A.E.M. and P.C.B.; visualization, M.H.; supervision, A.E.M.; project administration, A.E.M. and P.C.B.; funding acquisition, P.C.B. All authors have read and agreed to the published version of the manuscript.

**Funding:** This research was funded by the U.S. Department of State (DoS) Bureau of Diplomatic Security.

**Data Availability Statement:** Some or all data that were used, or generated, during the study are confidential in nature and may only be provided with restrictions.

**Acknowledgments:** The authors would like to thank U.S. State Department's Bureau of Diplomatic Research and Development branch, and the Energetic Materials Research and Testing Center (EMRTC) for their contributions to this research effort.

**Conflicts of Interest:** The authors declare no conflict of interest.

## References

1. Marchand, K.A.; Alfawakhiri, F. *Facts for Steel Buildings: Blast and Progressive Collapse*; AISC: Chicago, IL, USA, 2005.
2. *Single Degree of Freedom Structural Response Limits for Antiterrorism Design*; U.S. Army Corps of Engineers, Protective Design Center: Omaha, NE, USA, 2008.
3. Dusenberry, D.O. *Handbook for Blast-Resistant Design of Buildings*; Wiley: Hoboken, NJ, USA, 2010.
4. Haynes, J.R., Jr.; Pekelnicky, R.G.; Woodson, S.C.; Poland, C.D. *Blast-Resistance Benefits of Seismic Design—Phase 1 Study: Performance Analysis of Reinforced Concrete Strengthening Systems Applied to the Murrah Federal Building Design*; FEMA: Washington, DC, USA, 2005.
5. Pekelnicky, R.G.; Woodson, S.C.; Sweeny, S.C.; Haynes, J.R., Jr.; Magallanes, J.; Bonneville, D.R.; Poland, C.D. *Blast-Resistance Benefits of Seismic Design—Phase 2 Study: Performance Analysis of Structural Steel Strengthening Systems*; FEMA: Washington, DC, USA, 2010.
6. Hinman, E.E.; Hammond, D.J. *Lessons from the Oklahoma City Bombing—Defense Design Techniques*; ASCE: Reston, VA, USA, 1997.
7. Liew, J.R. Survivability of steel frame structures subject to blast and fire. *J. Constr. Steel Res.* **2008**, *64*, 854–866. [[CrossRef](#)]
8. Clough, L.G.; Clubley, S.K. Synergistic response of steel columns to explosive thermal and long duration blast loading. *Eng. Struct.* **2021**, *245*, 112944. [[CrossRef](#)]
9. Al-Thairy, H. Behaviour and Failure of Steel Columns Subjected to Blast Loads: Numerical Study and Analytical Approach. *Adv. Mater. Sci. Eng.* **2018**, *2018*, 1–20. [[CrossRef](#)]
10. Galal, M.A.; Bandyopadhyay, M.; Banik, A.K. Progressive Collapse Analysis of Three-Dimensional Steel–Concrete Composite Building due to Extreme Blast Load. *J. Perform. Constr. Facil.* **2020**, *34*, 04020021. [[CrossRef](#)]
11. Nassr, A.A.; Razaqpur, A.G.; Tait, M.J.; Campidelli, M.; Foo, S. Experimental Performance of Steel Beams under Blast Loading. *J. Perform. Constr. Facil.* **2012**, *26*, 600–619. [[CrossRef](#)]
12. Nassr, A.A.; Razaqpur, A.G.; Tait, M.J.; Campidelli, M.; Foo, S. Dynamic Response of Steel Columns Subjected to Blast Loading. *J. Struct. Eng.* **2014**, *140*, 04014036. [[CrossRef](#)]
13. Figuli, L.; Bedon, C.; Zvaková, Z.; Jangl, Š.; Kavický, V. Dynamic analysis of a blast loaded steel structure. *Procedia Eng.* **2017**, *199*, 2463–2469. [[CrossRef](#)]
14. Tyas, A.; Warren, J.A.; Bennett, T.; Fay, S. Prediction of clearing effects in far-field blast loading of finite targets. *Shock. Waves* **2011**, *21*, 111–119. [[CrossRef](#)]
15. Yussof, M.M.; Silalahi, J.H.; Kamarudin, M.K.; Chen, P.-S.; Parke, G.A.R. Numerical Evaluation of Dynamic Responses of Steel Frame Structures with Different Types of Haunch Connection Under Blast Load. *Appl. Sci.* **2020**, *10*, 1815. [[CrossRef](#)]
16. Weli, S.S.; Vigh, L.G. Blast Performance Evaluation of Steel Moment-Resisting Frame Equipped with Smart Bolted Connection. *J. Perform. Constr. Facil.* **2021**, *35*, 04021050. [[CrossRef](#)]
17. Nourzadeh, D.; Humar, J.; Braimah, A. Comparison of Response of Building Structures to Blast Loading and Seismic Excitations. *Procedia Eng.* **2017**, *210*, 320–325. [[CrossRef](#)]
18. Ibrahim, Y.E.; Nabil, M. Assessment of structural response of an existing structure under blast load using finite element analysis. *Alex. Eng. J.* **2019**, *58*, 1327–1338. [[CrossRef](#)]
19. McKay, A.; Bazan, M.; Gomez, M.; Marchand, K. *Steel Frame Structure Performance in Blast Environments—Task 2 Analysis and Final Reporting*; Protection Engineering Consultants: San Antonio, TX, USA, 2011.
20. ASCE. *Minimum Design Loads for Buildings and Other Structures (ASCE 7-10)*; ASCE/SEI 7-10; ASCE: Reston, VA, USA, 2010; Available online: <https://www.asce.org/asce-7/> (accessed on 1 September 2021).
21. ANSI/AISC. *Specification for Structural Steel Buildings (ANSI/AISC 360-10)*; American Institute of Steel Construction (AISC): Chicago, IL, USA, 2010.
22. Vulcraft. *Vulcraft Steel Roof and Floor Deck*; Vulcraft: Ancaster, ON, Canada, 2008.
23. ASTM International. *ASTM A992/A992M-11, Standard Specification for Structural Steel Shapes*; ASTM International: West Conshohocken, PA, USA, 2011.
24. ASTM International. *ASTM A500/A500M-10, Standard Specification for Cold-Formed Welded and Seamless Carbon Steel Structural Tubing in Rounds and Shapes*; ASTM International: West Conshohocken, PA, USA, 2010.
25. ASTM International. *ASTM A36/A36M-08, Standard Specification for Carbon Structural Steel*; ASTM International: West Conshohocken, PA, USA, 2008.
26. ASTM International. *ASTM A653/A653M-10, Standard Specification for Steel Sheet, Zinc-Coated (Galvanized) or Zinc-Iron Alloy Coated (Galvannealed) by Hot-Dip Process*; ASTM International: West Conshohocken, PA, USA, 2010.
27. ASTM International. *ASTM A325-10, Standard Specification for Structural Bolts, Steel, Heat Treated, 120/105 KSI Minimum Tensile Strength*; ASTM International: West Conshohocken, PA, USA, 2010.
28. ASTM International. *ASTM A615/A615M-09, Standard Specification for Deformed and Plain Carbon-Steel Bars for Concrete Reinforcement*; ASTM International: West Conshohocken, PA, USA, 2009.
29. International Code Council. *International Building Code (IBC)*; International Code Council: Falls Church, VA, USA, 2006.
30. Product Catalogue for 1600 WALL SYSTEMM1/SYSTEMM2 CURTAIN WALL. (n.d.). Available online: [www.kawneer.com](http://www.kawneer.com) (accessed on 1 September 2021).
31. ASCE. *Seismic Rehabilitation of Existing Buildings (ASCE 41-06)*; ASCE/SEI 41-06; ASCE: Reston, VA, USA, 2007.